1 **GATING-AFFECTING MUTATIONS IN *KCNK4* CAUSE A RECOGNIZABLE NEURODEVELOPMENTAL**

2 **SYNDROME**

3

4 Christiane K. Bauer,[1,*] Paolo Calligari,[2] Francesca Clementina Radio,[3] Viviana Caputo,[4]

5 Maria Lisa Dentici,[3] Nadia Falah,[5] Frances High,[6] Francesca Pantaleoni,[3] Sabina Barresi,[3]

6 Andrea Ciolfi,[3] Simone Pizzi,[3] Alessandro Bruselles,[7] Richard Person,[8] Sarah Richards,[8]

7 Megan T. Cho,[8] Daniela J. Claps Sepulveda,[3] Stefano Pro,[3] Roberta Battini,[9] Giuseppe

8 Zampino,[10] Maria Cristina Digilio,[3] Gianfranco Bocchinfuso,[2] Bruno Dallapiccola,[3] Lorenzo

9 Stella,[2] Marco Tartaglia[3,*]

10

11 [1]Center for Experimental Medicine, Institute of Cellular and Integrative Physiology, University

12 Medical Center Hamburg-Eppendorf, 20246 Hamburg, Germany.

13 [2]Department of Chemical Science and Technologies, University of Rome Tor Vergata, 00133

14 Rome, Italy.

15 [3]Genetics and Rare Diseases Research Division, Ospedale Pediatrico Bambino Gesù,

16 IRCCS, 00146 Rome, Italy.

17 [4]Department of Experimental Medicine, Sapienza University of Rome, 00161 Rome, Italy.

18 [5]Division of Clinical Genetics, Nemours Children's Hospital, Orlando, FL 32827, USA.

19 [6]Medical Genetics, Mass General Hospital for Children, Massachusetts General Hospital,

20 Boston, MA 02114-2696, USA.

21 [7]Department of Oncology and Molecular Medicine, Istituto Superiore di Sanità, 00161 Rome,

22 Italy.

23 [8]GeneDX, Gaithersburg, MD 20877, USA.

24 [9]Department of Developmental Neuroscience, IRCCS Stella Maris, 56128 Calambrone, Italy.

25 [10]Center for Rare Disease and Congenital Defects, Fondazione Policlinico Universitario A.

26 Gemelli, IRCCS, Università Cattolica del Sacro Cuore, 00168 Rome, Italy.

*corresponding authors:

Christiane Bauer, PhD
Institute of Cellular and Integrative Physiology
University Medical Center Hamburg-Eppendorf,
20246 Hamburg, Germany
Email: cbauer@uke.uni-hamburg.de
Phone: +49-40-741052183

Marco Tartaglia, PhD
Genetics and Rare Diseases Research Division
Ospedale Pediatrico Bambino Gesù, IRCCS
00146 Rome, Italy
Email: marco.tartaglia@opbg.net
Phone: +39-06-68593742

Email addresses:

Bauer CK	cbauer@uke.uni-hamburg.de
Calligari P	paolo.calligari@uniroma2.it
Radio FC	fclementina.radio@opbg.net
Caputo V	viviana.caputo@uniroma1.it
Dentici ML	marialisa.dentici@opbg.net
Falah N	falahnadia@gmail.com
High F	fhigh@partners.org
Pantaleoni F	francesca.pantaleoni@opbg.net
Barresi S	sabina.barresi@opbg.net
Ciolfi A	andrea.ciolfi@opbg.net
Pizzi S	simone.pizzi@opbg.net
Bruselles A	alessandro.bruselles@iss.it
Person R	rperson@genedx.com
Richards S	srichards@genedx.com
Cho MT	mcho@genedx.com
Bocchinfuso G	gianfranco.bocchinfuso@uniroma2.it
Claps Sepulveda DJ	dianelajudith.claps@opbg.net
Pro S	stefano.pro@opbg.net
Battini R	roberta.battini@fsm.unipi.it
Zampino G	giuseppe.zampino@unicatt.it
Digilio MC	digilio@opbg.net
Dallapiccola B	bruno.dallapiccola@opbg.net
Stella L	stella@stc.uniroma2.it
Tartaglia M	marco.tartaglia@opbg.net

ABSTRACT

Aberrant activation or inhibition of potassium (K$^+$) currents across the plasma membrane of cells has been causally linked to altered neurotransmission, cardiac arrhythmias, endocrine dysfunction, and perturbed developmental processes, more rarely. The K$^+$~~potassium~~ channel subfamily K member 4 (KCNK4), also known as TRAAK (TWIK-related arachidonic acid-stimulated K$^+$ channel), belongs to the mechano-gated ion channels of the TRAAK/TREK subfamily of two-pore-domain (K2P) K$^+$ channels. While K2P channels are well-known to contribute to the resting membrane potential and cellular excitability, their involvement in pathophysiological processes remains largely uncharacterized. We report that *de novo* missense mutations in *KCNK4* cause a recognizable syndrome with a distinctive facial gestalt, for which we propose the acronym FHEIG (*f*acial dysmorphism, *h*ypertrichosis, *e*pilepsy, *i*ntellectual disability/developmental delay, and *g*ingival overgrowth)~~with major features including distinctive facial gestalt, gingival overgrowth, hypertrichosis, intellectual disability, and epilepsy~~. Patch-clamp analyses documented an impressive gain-of-function of the identified KCNK4 channel mutants basally, and impaired ~~mechano~~sensitivity to mechanical stimulation and arachidonic acid. Co-expression experiments ~~provided evidence of the~~ indicated a dominant behavior of the disease-causing mutations. Remarkably, molecular dynamics simulations consistently indicated that mutations favor sealing of the lateral intramembrane fenestration that has been proposed to negatively control K$^+$ flow by allowing lipid access to the central cavity of the channel. Overall, our findings illustrate the pleiotropic effect of dysregulated KCNK4 function, and provide support to the hypothesis of a gating mechanism based on the lateral fenestrations of K2P channels.

The human genome contains almost 80 genes encoding ~~for~~ potassium (K$^+$) channels, which

constitute the most diversified class of ion channels with regard to structure and gating

characteristics (see OMIM database). Such diversity allows K$^+$ channels to serve various

functions in both excitable and non-excitable cells.[1-3] K$^+$ channels contribute to the

maintenance and stabilization of the resting membrane potential, help to repolarize action

potentials, mediate hyperpolarization, and determine cellular electrical activity or even cell

proliferation. Moreover, K$^+$ channels also efficiently mediate modulations of membrane

potential and cell function by controlling the K$^+$ flux through the cell membrane in response of

multiple signals. Since ~~the key role of~~ the membrane potential has a key role in the control of

a wide array of cellular processes, including cellular excitability, neurotransmitter release,

hormone secretion, and electrolyte transport, it is not surprising that aberrant or impaired K$^+$

flux due to hyperactivating or inactivating mutations in genes coding for K$^+$ channels

underlies a heterogeneous spectrum of human disorders affecting neurotransmission and

central nervous system function, cardiac electrophysiology, hormone secretion, and kidney

function.[2,4-6] Remarkably, the aberrant function of some of these channels has recently been

documented to ~~play pleiotropic effect on physiological processes as well as to~~ affect

development and underlie syndromic disorders.[7-11] Here, we report on the identification of

dominantly acting mutations in *KCNK4* (~~O~~MIM: 605720), which encodes a two-pore-domain

(K2P) K$^+$ channel,[12-14] as the cause of a previously unrecognized syndrome having a

distinctive facial gestalt, gingival overgrowth, hypertrichosis, intellectual disability, and

epilepsy, as major features. KCNK4, also known as TRAAK (TWIK-related arachidonic acid-

stimulated K$^+$ channel), is one of three lipid- and mechano-sensitive K2P channels

constituting the TRAAK/TREK subfamily. We provide data indicating that the disease-causing

mutations are activating basally, and cause impaired ~~mechano~~sensitivity to mechanical

stimuli and arachidonic acid. Finally, we offer molecular dynamics data suggesting the

1 structural mechanism by which these mutations exert their gain of function, providing support

2 to the hypothesis of a gating mechanism based on the lateral fenestrations of K2P channels.

3 In the frame of a research program dedicated to individuals affected by undiagnosed

4 ~~patients~~ diseases performed at the Ospedale Pediatrico Bambino Gesù, Rome, the exomes

5 of two unrelated subjects with a molecularly unexplained, clinically superimposable

6 phenotype were scanned to identify the underlying molecular cause. Clinical data and DNA

7 samples were collected from the participating families after written informed consent was

8 obtained, and stored and used following the Institutional Review Board recommendations. In

9 both children, the unusual core of features included variable developmental delay~~/intellectual~~

10 ~~disability (ID)~~, distinctive facies, gingival overgrowth, hypertrichosis, and EEG

11 anomalies/epilepsy (Figure 1, Table 1, Supplemental Note). Whole-exome sequencing

12 (WES) used DNA samples obtained from leukocytes. Exome capture was attained using the

13 SureSelect Clinical Research Exome V.2 (subject 1) and Nextera V.1.2 (subject 2 and both

14 parents) target enrichment kits, and sequencing was performed on a NextSeq500, using

15 paired-end. WES data processing, sequence alignment to GRCh37, and variant filtering and

16 prioritization by allele frequency, predicted functional impact, and inheritance models were

17 performed using an in-house implemented pipeline, as previously described.[15-17] Briefly,

18 reads were aligned to human genome build GRCh37/UCSC hg19, and variants were quality-

19 filtered according to GATK's 2016 best practices, annotated, and filtered against public

20 (dbSNP150 and gnomAD V.2.0) and in-house (>1,300 population-matched exomes)

21 databases to retain private and rare (unknown frequency or MAF <0.1%) variants located in

22 exons with any effect on the coding sequence, and within splice site regions. The functional

23 impact of variants was analyzed by Combined Annotation Dependent Depletion (CADD)

24 V.1.3, M-CAP V.1.0, and InterVar V.0.1.6 algorithms,[18-20] to obtain clinical interpretation

25 according to ACMG 2015 guidelines.[21] WES data output is reported in Table S1. Two

26 variants in *KCNK4* (subject 1: NM_001317090.1:c.515C>A, p.Ala172Glu; subject 2:

NM_001317090.1:c.730G>C, p.Ala244Pro), compatible with autosomal dominant

transmission of the trait, were identified as the only shared events. Both variants were

confirmed to occur as *de novo* events by Sanger sequencing. STR analysis confirmed

paternity in family 1, and mutation analysis performed on primary skin fibroblasts and hair

bulb epithelial cells of both affected subjects supported the germline origin of mutations. One

additional subject born to unaffected parents, sharing a similar gestalt, intellectual disability

(ID) and epilepsy, and carrying the previously identified NM_001317090.1:c.515C>A as a *de*

novo event in the same gene, was found by using the web tool GeneMatcher.[22] In this

subject, targeted enrichment was attained using the IDT xGen Exome Research Panel v1.0

(affected subject and both parents), and sequencing performed using a HiSeq4000 platform

(Table S1). WES data analysis was performed as previously reported,[23] taking into account

the general assertion criteria for variant classification available on the GeneDx ClinVar

submission page (http://www.ncbi.nlm.nih.gov/clinvar/submitters/submitter code 26957).

Variant validation was confirmed by Sanger sequencing. The two variants had not been

reported in ExAC/gnomAD, affected residues are conserved among vertebrate orthologs,

with Ala[244] invariantly occurring among members of the TRAAK/TREK subfamily (Figure S1),

and were predicted to have a damaging impact on protein function by CADD and M-CAP

algorithms (Table S1). In all subjects, WES data analysis excluded the presence of

functionally relevant variants compatible with known Mendelian conditions based on the

expected inheritance model and clinical presentation (Table S2).

K2P channels are dimeric, with each subunit contributing two pore domains to the

channel (Figure 2A).[13,14,24] Based on available structures of KCNK4, both affected residues

mapped in regions possibly involved in KCNK4 activation,[25-29] with Ala[244] located at the

center of helix M4, and Ala[172] in M3, in a region of the helix with extensive interaction with

M2. Different models of TRAAK/TREK channel gating have been proposed.[24,27,30-32]

According to one hypothesis, channel opening appears to be mediated by a conformational

transition of helices M4, causing the closing of two lateral fenestrations exposing the ion-conduction pathway to the hydrophobic core of the lipid membrane.[27,33] When M4 is straight ("down" state) (Figure 2B) lipid moieties can insert in the lateral fenestration, thus blocking K^+ flow (inactive conformation). Bending of M4 ("up" conformation) closes the fenestrations, preventing lipid insertion, and leading to a conducting state of the channel.[27] In alternative models, channel activation involves conformational transitions at the selectivity filter.[24] However, the possibility that multiple mechanisms may contribute to the control of K^+ flux in response of different stimuli cannot be ruled out. To explore the structural consequences of the p.Ala172Glu and p.Ala244Pro substitutions, molecular dynamics simulations were performed (Supplemental methods), starting from the structure of wild-type KCNK4 with one of the M4 helices (M4_B) in the "up" state (PDB code 4WFE).[27] embedded in a lipid bilayer. Positions of missing residues and the identified amino acid substitutions were modeled using a standard protocol of energy minimization and simulated annealing,[34] implemented in the Modeller 9.18 software.[35] MD simulations (Supplemental methods) were performed using the GROMACS simulation package,[36] and the CHARMM36 force-field.[37] Long-range electrostatic interactions were calculated using the particle mesh Ewald method,[38] and the cut-off distance for the non-bonded interaction was set equal to 12.0 Å. The channels were simulated in a lipid bilayer comprising 201 1-palmitoyl,2-oleoyl-*sn*-glycero-3-phosphocholine (POPC) molecules, in the presence of ~40000 TIP3P,[39] water molecules, and K^+ and Cl^- ions in order to ensure system neutrality and an ion concentration of 0.15 M. After an equilibration protocol (Supplemental methods), a 100 ns production run was performed for each system. In agreement with the lateral fenestration-based model of gating, during the trajectory performed in the absence of channel-activating stimuli, the M4_B helix of the wild-type (WT) protein evolved towards the "down" conformation (the same straight structure was maintained for the M4_A helix) (Figure S2). "Down" conformations were populated by both helices also in the p.Ala172Glu mutant. By contrast, in the p.Ala244Pro channel both helices attained an

"up" conformation, in agreement with the helix-breaking properties of Pro residues.[34] The effect of the amino acid substitutions on the opening/closing of lateral fenestrations was also investigated. The lateral fenestrations were significantly less open in the p.Ala244Pro and p.Ala172Glu mutants compared to the ~~wild-type~~WT protein (Figure 2C). By taking a reference value of 2 Å (*i.e.*, the size of a methane molecule to represent the size of a lipid chain) as cut-off, the lateral fenestrations of ~~wild type~~WT, p.Ala172Glu, and p.Ala244Pro structures were open for 27%, 12%, and 0.2% of the time, respectively. In the model of gating based on lateral fenestrations, this finding suggests basal activation in both mutants. By contrast, no significant differences were observed in the selectivity filter region (Figure S3). Remarkably, in the simulation of p.Ala172Glu, the lateral fenestrations were closed for a significant fraction of the trajectory, even though both helices were in the "down" conformation (Figure 2C), suggesting that sealing of the lateral openings is more complex than simple helix bending.[27] This occlusion resulted from the formation of a hydrophobic cluster involving the side chains of Leu^{125}, Phe^{246} and Leu^{250}. In the p.Ala172Glu mutant, the substitution induced the formation of an inter-domain salt bridge between Glu^{172} (M3 helix) and Arg^{147} (M2 helix) (Figure S4). The strengthened salt bridge network between the M2 and M3 helices might be responsible for the closing of the fenestration, due to the multiple interactions among helices M2, M3 and M4.

To investigate experimentally the predicted activating effect of the two identified *KCNK4* mutations, their impact on protein function was ~~Functional consequences of the identified KCNK4 mutations were~~ assessed by patch-clamp experiments (Supplemental Methods) in transfected Chinese hamster ovary (CHO) cells. Nucleotide substitutions resulting in the p.Ala244Pro and p.Ala172Glu amino acid changes were introduced into the *KCNK4* cDNA (clone KT4.1a) cloned in a pcDNA3 vector (Invitrogen), using the QuikChange Site-Directed Mutagenesis Kit (Agilent Technologies). Cells were transfected with ~~wild-type (~~WT~~)~~ or mutant human KCNK4 cDNA (400 ng/ml or 80 ng/ml as final concentration; co-expression assays:

80 ng/ml, each channel plasmid, resulting in a total of 160 ng/ml channel cDNA), and cDNA

encoding EGFP-N1 (Clontech), using Lipofectamine 2000 (Invitrogen). In the whole-cell

mode, we recorded outward-rectifying currents in cells expressing ~~wild-type~~WT KCNK4,

which became evident at positive potentials. Membrane currents recorded from cells

transfected with the mutant channels were much larger and already prominent in the negative

potential range (Fig. 3A,B). p.Ala244Pro KCNK4 channels mostly lacked a voltage-

dependent initial current increase, resembling maximally stimulated ~~wild-type~~WT KCNK4

channels.[32] Voltage ramps were used to evaluate current amplitude at 0 mV and

conductance at -80 mV, encompassing the most important physiological voltage range.

Expression of the mutant KCNK4 channels, as well as their co-expression with ~~wild-type~~WT

KCNK4, resulted in significantly increased current amplitudes compared to ~~wild-type~~WT

channels (Figure 3C,D, and Figure S5), documenting the dominant impact of mutations.

Current reversal was close to -80 mV and demonstrated preserved K^+ selectivity of both

mutant channels. Since the whole-cell mode is regarded as the only configuration of the

patch clamp-technique that exerts no tension on the cell membrane,[35] the observed

differences reflect an impressive gain-of-function of the mechanically unstimulated KCNK4

channel induced by both point mutations.

Mechanosensitivity of the different KCNK4 channels was investigated in outside-out

experiments. ~~Wild-type~~WT KCNK4 channels were activated by positive pressure applied

through the patch pipette, and the effect often increased with repetitive stimulation and with

time (Figure 4A,B). Maximal activation resulted in an increase in current amplitudes to almost

hundredfold of the initial value (Figure 4C,D). In most experiments, the K^+ current generated

by maximally activated ~~wild-type~~WT KCNK4 channels in the small membrane patch

exceeded the amplitude of the corresponding whole-cell current. Outside-out patches from

cells expressing each of the KCNK4 mutants exhibited higher initial current amplitude at 0

mV and higher basal K^+ conductance. Remarkably, the effect of pressure stimulation was

significantly impaired in patches containing these mutants (Figure 4, Figure S6). Pressure-induced changes in current amplitude were absent in most experiments on p.Ala244Pro KCNK4 channels, and only a small increase in current amplitude with pressure application was documented for the p.Ala172Glu mutant. Coexpression experiments with ~~wild-type~~WT and p.Ala172Glu KCNK4 channels resulted in slightly more pronounced pressure-induced channel activation, but the effects were significantly smaller than for the ~~wild-type~~WT channels (Figure S6C).

In addition to their mechanosensitivity, K2P channels of the TRAAK/TREK subfamily are sensitive to certain lipids.[12,13] Specifically, KCNK4 is activated by arachidonic acid and polyunsaturated fatty acids. Accordingly, application of a high concentration of arachidonic acid (20 µM) resulted in a huge increase in WT KCNK4 currents recorded in the whole-cell configuration (Figure 5A,D). Using the identical experimental approach, both KCNK4 mutants were found to lack the impressive channel activation in response to arachidonic acid (Figure 5B,C,D), which likely reflects their maximal activation basally.

Measurements in the cell-attached configuration with undisturbed intracellular *milieu* and intact cytoskeleton gave qualitatively similar results (Figure S7A-C), further supporting the gain-of-function of the unstimulated mutant channels and their impaired mechanosensitivity. Of interest, the *I/V* relation showed pronounced inward rectification in most cell-attached measurements with the p.Ala244Pro mutant, while this feature was rarely (p.Ala172Glu) or never (~~wild-type~~WT) observed in cells expressing the other KCNK4 channels (Figure S7D,E). As inward rectification of activated KCNK channels with inverted K^+ concentration gradient has been reported,[32] the degree of inward rectification is likely to mirror the level of intracellular K^+ depletion. Deleterious effects of substantial K^+ loss associated with high p.Ala244Pro KCNK4 expression levels are suggested by a lack of cells with bright EGFP fluorescence (Figure S7F). This "negative selection" most probably biased the results of the electrophysiological measurements leading to an underestimation of the

channel-activating effect promoted by the p.Ala244Pro substitution. Overall, the functional

data are in agreement with the MD findings, and similarly to mechanical stimulation,[27,28,31]

both mutations are suggested to result in enhanced closing of the lateral fenestrations,

favoring channel opening. This can readily explain the high basal activity, as well as the

impaired mechanosensitivity of the mutant channels. Of note, also arachidonic acid failed to

activate the disease-causing mutant channels, suggesting that both mutations promote

activation of the channel basally, which cannot be further increased by stimuli involving a

similar mechanism of channel activation.

While the role of K2P channels in controlling the membrane potential makes them as

potential players in a wide array of cellular processes, only subtle alterations in physiologic

processes have been linked to dysfunction of these channels.[36] Our findings provide

evidence that gain-of-function mutations in *KCNK4* cause a distinctive neurodevelopmental

syndrome, for which we propose the acronym FHEIG (*f*acial dysmorphism, *h*ypertrichosis,

*e*pilepsy, *i*ntellectual disability/developmental delay, and *g*ingival overgrowth). While

additional cases are required to delineate more accurately the clinical variability associated

with activating *KCNK4* mutations, the specific association of features and distinctive facies

support the view that this condition represents a novel nosologic entity. Remarkably, the

cardinal features characterizing this disorder are reminiscent of the phenotypic continuum

associated with activating mutations in the voltage-gated K$^+$ channel *KCNH1* (MIM:

603305),[8,9] and disorders caused by mutations in *ABCC9* (MIM: 601439) and *KCNJ8* (OMIM:

600935), two genes encoding ATP-sensitive potassium channel subunits with defective

function in Cantù syndrome.[10,11] In FHEIG syndrome, tThe clinical phenotype is characterized

by a significant evolution of the craniofacial features with age and should be considered in

differential diagnosis with other disorders (Table S2). Neonatally, it resembles Wiedemann-

Steiner syndrome (OMIM: 605130) to some extent, while later the phenotype becomes more

similar to Temple-Baraitser syndrome (OMIM: 611816) and mild forms of Cantù (OMIM:

11

239850) and Coffin-Siris (OMIM: 135900) syndromes. Similarly to what observed in these syndromes, the three affected subjects with *de novo KCNK4* mutations show variable developmental delay and cognitive impairment, ranging from a mild speech delay and disorganized pattern of development (individual 2) to an extremely severe ID (individual 1). In contrast to other K2P channels, KCNK4 appears to be almost exclusively expressed in neuronal cells of the central and peripheral nervous system, and retina (see GTEx database); so, the finding of its pleiotropic impact is unexpected. In rodent peripheral somatosensory neurons, KCNK4 appears to modulate thermo- and mechano-sensation and the respective threshold to nociception.[37] Laser-evoked potentials assessed in subjects 1 and 2 did not provide any aberrant pattern, suggesting no gross dysregulation of temperature and pressure sensitivity.

Depending upon the gating behavior of a given K^+ channel and its cellular and subcellular expression profile in the brain, intellectual impairment and seizures can result from either loss-of function or gain-of-function mutations.[2,5,7-11,38] Remarkably, gingival overgrowth is a major feature in ~~patients~~ subjects with gain-of-function mutations in *KCNH1*,[8,9] *KCNQ1*,[39] and *KCNK4* (present study), which consistently result in significantly elevated K^+ conductance at more negative potentials. Of note, Kcnk4$^{-/-}$ mice exhibit neither obvious developmental abnormalities ~~and~~ nor increased susceptibility to seizures, ~~nor~~ deficits in cognition, touch, vision and hearing.[40] Thus, loss of KCNK4 function is likely compensated for by other members of the K2P family or its relevance is limited to pathophysiological conditions like brain ischemia.[41,42] Accordingly, the two disease-causing *KCNK4* mutations resulted in an impressive gain of function, indicated by a dramatically increased basal K^+ conductance. Of note, the sustained high K^+ conductance responsible for the clinical features and symptoms observed in FHEIG syndrome is expected to drain K^+ out of cells that exhibit considerable depolarizing currents.~~neurons,~~ This can result in intracellular K^+ depletion and increased interstitial K^+ concentration, with a depolarizing effect also on neighboring cells.

Taken together, our findings document a novel channelopathy induced by hyperactivation of KCNK4 channels. While the molecular mechanisms controlling K2P channel function are still object of debate, the present *in silico* and *in vitro* data consistently support the relevance of the closing of lateral fenestrations to channel gating,[24,43] and suggest that helix bending is not the only conformational transition controlling the state of lateral fenestrations in K2P channels.

Supplemental Data

Supplemental data include supplemental methods, ~~supplemental clinical data~~case reports, seven figures, and three tables.

WEB resources

OMIM, http://www.omim.org ~~https://www.ncbi.nlm.nih.gov/omim/~~

gnomAD browser, http://gnomad.broadinstitute.org

CADD, http://cadd.gs.washington.edu

M-CAP, http://bejerano.stanford.edu/mcap/

GTEx database, https://www.gtexportal.org/home/

InterVar, http://wintervar.wglab.org/

ClinVar database, https://www.ncbi.nlm.nih.gov/clinvar/

References

1   Hille, B. (2001). Ion channels of excitable membranes. (Sinauer Associates).

2   Tian, C., Zhu, R., Zhu, L., Qiu, T., Cao, Z., and Kang, T. (2014). Potassium channels: structures, diseases, and modulators. Chem. Biol. Drug Des. 83, 1-26.

3   Urrego, D., Tomczak, A.P., Zahed, F., Stühmer, W., and Pardo, L.A. (2014). Potassium channels in cell cycle and cell proliferation. Philos. Trans. R. Soc. Lond. B Biol. Sci. 369, 20130094.

4   Shieh, C.C., Coghlan, M., Sullivan, J.P., and Gopalakrishnan, M. (2000). Potassium channels: molecular defects, diseases, and therapeutic opportunities. Pharmacol. Rev. 52, 557-594.

5   Jentsch, T.J. (2000). Neuronal KCNQ potassium channels: physiology and role in disease. Nat. Rev. Neurosci. 1, 21-30.

6   Chiamvimonvat, N., Chen-Izu, Y., Clancy, C.E., Deschenes, I., Dobrev, D., Heijman, J., Izu, L., Qu, Z., Ripplinger, C.M., Vandenberg, J.I., et al. (2017). Potassium currents in the heart: functional roles in repolarization, arrhythmia and therapeutics. J. Physiol. 595, 2229-2252.

7   Bockenhauer, D., Feather, S., Stanescu, H.C., Bandulik, S., Zdebik, A.A., Reichold, M., Tobin, J., Lieberer, E., Sterner, C., Landoure, G., et al. (2009). Epilepsy, ataxia, sensorineural deafness, tubulopathy, and KCNJ10 mutations. N. Engl. J. Med. 360, 1960-1970.

8   Simons, C., Rash, L.D., Crawford, J., Ma, L., Cristofori-Armstrong, B., Miller, D., Ru, K., Baillie, G.J., Alanay, Y., Jacquinet, A, et al. (2015). Mutations in the voltage-gated potassium channel gene KCNH1 cause Temple-Baraitser syndrome and epilepsy. Nat. Genet. 47, 73-77.

9   Kortüm, F., Caputo, V., Bauer, C.K., Stella, L., Ciolfi, A., Alawi, M., Bocchinfuso, G., Flex, E., Paolacci, S., Dentici, M.L., et al. (2015). Mutations in KCNH1 and ATP6V1B2 cause Zimmermann-Laband syndrome. Nat. Genet. 47, 661-667.

10 Harakalova, M., van Harssel, J.J., Terhal, P.A., van Lieshout, S., Duran, K., Renkens, I., Amor, D.J., Wilson, L.C., Kirk, E.P., Turner, C.L., et al. (2012). Dominant missense mutations in ABCC9 cause Cantú syndrome. Nat. Genet. 44, 793-796.

11. Cooper, P.E., Reutter, H., Woelfle, J., Engels, H., Grange, D.K., van Haaften, G., van Bon, B.W., Hoischen, A., and Nichols, C.G. (2014). Cantú syndrome resulting from activating mutation in the KCNJ8 gene. Hum. Mutat. 35, 809-813.

12 Fink, M., Lesage, F., Duprat, F., Heurteaux, C., Reyes, R., Fosset, M., and Lazdunski, M. (1998). A neuronal two P domain K+ channel stimulated by arachidonic acid and polyunsaturated fatty acids. EMBO J. 17, 3297-3308.

13 Feliciangeli, S., Chatelain, F.C., Bichet, D., and Lesage, F. (2015). The family of K_{2P} channels: salient structural and functional properties. J. Physiol. 593, 2587-2603.

14 Sepúlveda, F.V., Pablo Cid, L., Teulon, J., and Niemeyer, M.I. (2015). Molecular aspects of structure, gating, and physiology of pH-sensitive background K_{2P} and K_{ir} K+-transport channels. Physiol. Rev. 95, 179-217.

15   Niceta, M., Stellacci, E., Gripp, K.W., Zampino, G., Kousi, M., Anselmi, M., Traversa, A., Ciolfi, A., Stabley, D., Bruselles, A., et al. (2015). Mutations Impairing GSK3-Mediated MAF Phosphorylation Cause Cataract, Deafness, Intellectual Disability, Seizures, and a Down Syndrome-like Facies. Am. J. Hum. Genet. 96, 816-825.

16   Flex, E., Niceta, M., Cecchetti, S., Thiffault, I., Au, M.G., Capuano, A., Piermarini, E., Ivanova, A.A., Francis, J.W., Chillemi, G., et al. (2016). Biallelic Mutations in TBCD, Encoding the Tubulin Folding Cofactor D, Perturb Microtubule Dynamics and Cause Early-Onset Encephalopathy. Am. J. Hum. Genet. 99, 962-973.

17   Sferra, A., Baillat, G., Rizza, T., Barresi, S., Flex, E., Tasca, G., D'Amico, A., Bellacchio, E., Ciolfi, A., Caputo, V. et al. (2016). TBCE Mutations Cause Early-Onset Progressive Encephalopathy with Distal Spinal Muscular Atrophy. Am. J. Hum. Genet. 99:974-983.

18   Kircher, M., Witten, D.M., Jain, P., O'Roak, B.J., Cooper, G.M., and Shendure, J. (2014). A general framework for estimating the relative pathogenicity of human genetic variants. Nat. Genet. 46, 310-315.

19   Jagadeesh, K.A., Wenger, A.M., Berger, M.J., Guturu, H., Stenson, P.D., Cooper, D.N., Bernstein, J.A., and Bejerano, G. (2016). M-CAP eliminates a majority of variants of uncertain significance in clinical exomes at high sensitivity. Nat. Genet. 48, 1581-1586.

20   Li, Q., and Wang, K. (2017). InterVar: Clinical Interpretation of Genetic Variants by the 2015 ACMG-AMP Guidelines. Am. J. Hum. Genet. 100, 267-280.

21   Richards, S., Aziz, N., Bale, S., Bick, D., Das, S., Gastier-Foster, J., Grody, W.W., Hegde, M., Lyon, E., Spector, E., et al. (2015). Standards and guidelines for the interpretation of sequence variants: a joint consensus recommendation of the American College of Medical Genetics and Genomics and the Association for Molecular Pathology. Genet. Med. 17, 405-424.

22 Sobreira, N., Schiettecatte, F., Valle, D., and Hamosh, A. (2015). GeneMatcher: a matching tool for connecting investigators with an interest in the same gene. Hum. Mutat. 36, 928-930.

23 Tanaka, A.J., Cho, M.T., Millan, F., Juusola, J., Retterer, K., Joshi, C., Niyazov, D., Garnica, A., Gratz, E., Deardorff, M., et al. (2015). Mutations in SPATA5 Are Associated with Microcephaly, Intellectual Disability, Seizures, and Hearing Loss. Am. J. Hum. Genet. 97, 457-464.

24 Renigunta, V., Schlichthörl, G., and Daut, J. (2015). Much more than a leak: structure and function of K_{2P}-channels. Eur. J. Physiol. 467, 867-894.

25 Brohawn, S.G., del Marmol, J., and MacKinnon, R. (2012). Crystal structure of the human K2P TRAAK, a lipid- and mechano-sensitive K^+ ion channel. Science 335, 436-441.

26 Brohawn, S.G., Campbell, E.B., and MacKinnon, R. (2013). Domain-swapped chain connectivity and gated membrane access in a Fab-mediated crystal of the human TRAAK K+ channel. Proc. Natl. Acad. Sci. U S A 110, 2129-2134.

27 Brohawn, S.G., Campbell, E.B., and MacKinnon, R. (2014). Physical mechanism for gating and mechanosensitivity of the human TRAAK K+ channel. Nature 516, 126-130.

28 Brohawn, S.G. (2015). How ion channels sense mechanical force: insights from mechanosensitive K2P channels TRAAK, TREK1, and TREK2. Ann N Y Acad. Sci. 1352, 20-32.

29 Lolicato, M. Riegelhaupt, P.M., Arrigoni, C., Clark, K.A., and Minor, D.L. Jr. (2014). Transmembrane helix straightening and buckling underlies activation of mechanosensitive and thermosensitive K(2P) channels. Neuron 84, 1198-1212.

30 Niemeyer, M.I., Cid, L.P., González, W., and Sepúlveda, F.V. (2016). Gating, regulation, and structure in K_{2P} K^+ channels: In varietate concordia? Mol. Pharmacol. 90, 309-317.

31   Aryal, P., Jarerattanachat, V., Clausen, M.V., Schewe, M., McClenaghan, C., Argent, L., Conrad, L.J., Dong, Y.Y., Pike, A.C.W., Carpenter, E.P., et al. (2017). Bilayer-mediated structural transitions control mechanosensitivity of the TREK-2 K2P channel. Structure 25, 708-718.e2.

32   Schewe, M., Nematian-Ardestani, E., Sun, H., Musinszki, M., Cordeiro, S., Bucci, G., de Groot, B.L., Tucker, S.J., Rapedius, M., and Baukrowitz, T. (2016). A Non-canonical Voltage-Sensing Mechanism Controls Gating in K2P K^+ Channels. Cell 164, 937-949.

33   Masetti, M., Berti, C., Ocello, R., Di Martino, G.P., Recanatini, M., Fiegna, C., and Cavalli A. (2016). Multiscale simulations of a two-pore potassium channel. J. Chem. Theory Comput. 12, 5681-5687.

34   Fiser, A., Do, R.K.G., and Šali, A. (2000). Modeling of loops in protein structures. Protein Sci. 9, 1753-1773.

35   Šali, A., and Blundell, T.L. (1993). Comparative Protein Modelling by Satisfaction of Spatial Restraints. J. Mol. Biol. 234, 779-815.

36   Abraham, M.J., Murtola, T., Schulz, R., Páll, S., Smith, J.C., Hess, B., and Lindahl, E. (2015). GROMACS: High performance molecular simulations through multi-level parallelism from laptops to supercomputers. SoftwareX 1-2, 19-25.

37   Huang, J., and MacKerell, A.D. (2013). CHARMM36 all-atom additive protein force field: Validation based on comparison to NMR data. J. Comp. Chem. 34, 2135-2145.

38   Darden, T., York, D., and Pedersen, L. (1993). Particle mesh Ewald: An N· log (N) method for Ewald sums in large systems. J. Chem. Phys. 98, 10089-10092.

39   Jorgensen, W. L., Chandrasekhar, J., Madura, J. D., Impey, R. W., and Klein, M. L. (1983). Comparison of simple potential functions for simulating liquid water. J. Chem. Phys. 79, 926-935.

34   Bobone, S., Bocchinfuso, G., Park, Y., Palleschi, A., Hahm, K.S., and Stella, L. (2013). The importance of being kinked: role of Pro residues in the selectivity of the helical antimicrobial peptide P5. J. Peptide Sci. 19, 758-769.

35   Schmidt, D., del Mármol, J., and MacKinnon, R. (2012). Mechanistic basis for low threshold mechanosensitivity in voltage-dependent K+ channels. Proc. Natl. Acad. Sci. U S A 109, 10352-10357.

36   Sabbadini, M., and Yost, C.S. (2009). Molecular biology of background K channels: insights from K_{2P} knockout mice. J. Mol. Biol. 385, 1331-1344.

37   Noël, J., Zimmermann, K., Busserolles, J., Deval, E., Alloui, A., Diochot, S., Guy, N., Borsotto, M., Reeh, P., Eschalier, A., and Lazdunski, M. (2009). The mechano-activated K+ channels TRAAK and TREK-1 control both warm and cold perception. EMBO J. 28, 1308-1318.

38   Lehman, A., Thouta, S., Mancini, G.M.S., Naidu, S., van Slegtenhorst, M., McWalter, K., Person, R., Mwenifumbo, J., Salvarinova, R., CAUSES Study, et al. (2017). Loss-of-Function and Gain-of-Function Mutations in KCNQ5 Cause Intellectual Disability or Epileptic Encephalopathy. Am. J. Hum. Genet. 101, 65-74.

39   Tommiska, J., Känsäkoski, J., Skibsbye, L., Vaaralahti, K., Liu, X., Lodge, E.J., Tang, C., Yuan, L., Fagerholm, R., Kanters, J.K., et al. (2017). Two missense mutations in KCNQ1 cause pituitary hormone deficiency and maternally inherited gingival fibromatosis. Nat. Commun. 8, 1289.

40   Heurteaux, C., Guy, N., Laigle, C., Blondeau, N., Duprat, F., Mazzuca, M., Lang-Lazdunski, L., Widmann, C., Zanzouri, M., Romey, G., and Lazdunski, M. (2004). TREK-1, a K+ channel involved in neuroprotection and general anesthesia. EMBO J. 23, 2684-2695.

41 Laigle, C., Confort-Gouny, S., Le Fur, Y., Cozzone, P.J., and Viola, A. (2013). Deletion of TRAAK potassium channel affects brain metabolism and protects against ischemia. PLoS One 7, e53266.

42 Mirkovic, K., Palmersheim, J., Lesage, F., and Wickman, K. (2012). Behavioral characterization of mice lacking Trek channels. Front. Behav. Neurosci. 10.3389/fnbeh.2012.00060.

43 McClenaghan, C., Schewe, M., Aryal, P., Carpenter, E.P., Baukrowitz, T., Tucker, S.J. (2016). Polymodal activation of the TREK-2 K2P channel produces structurally distinct open states. J. Gen. Physiol. 147, 497-505.

Table 1. Clinical features of the three subjects with de novo *KCNK4* mutations.

~~Patient~~	Subject 1	Subject 2	Subject 3
Sex	M	M	F
Age at last evaluation	11 m	5 yrs 7 m	8 yrs
***KCNK4* mutation** (NM_001317090.1)	c.515C>A (p.Ala172Glu)	c.730G>C (p.Ala244Pro)	c.515 C>A (p.Ala172Glu)
Inheritance	simplex case, *de novo*	simplex case, *de novo*	simplex case, *de novo*
Pregnancy history	uneventful	uneventful	uneventful
Neonatal course			
Feeding/swallowing problems	+	-	+
Growth (at birth)			
Gestational age	at term	at term	at term
Height	54cm (75th-90th)	49cm (25th-50th)	52.07cm (75th)
Weight	3,925g (50th-75th)	3,030g (25th-50th)	3,580g (50th-75th)
OFC	34cm (50th-75th)	34cm (50th-75th)	not available
Growth (at last evaluation)			
Height	78 cm (90th-97th)	104cm (50th)	117.7cm (10th)
Weight	9.0kg (25th-50th)	15.5kg (10th)	21.6Kg (10th)
OFC	43.5cm (3rd-10th)	51.2cm (25th)	51.5cm (10th)
Development delay			
Global developmental delay	+[1]	mild speech delay[2]	+[3]
Intellectual disability	~~moderate~~ severe	low average	severe
IQ (scale)	not applicable	85 (Griffiths)	not available
Gross motor skills	delayed	not delayed	delayed
Fine motor skills	not applicable	delayed	delayed
Language delay	not applicable	mild	+
Abnormal behavior	not applicable	-	+
Neurological features			
Seizures/EEG anomalies	EEG anomalies	Right focal clonic seizure with secondary generalization	tonic clonic seizure
Hypotonia	+	-	+
Hyperreflexia	+	-	not available
Intention tremor	-	-	+
Visual impairment	nystagmus with bilateral optic hypoplasia	-	nystagmus with bilateral optic hypoplasia
Craniofacial			
Bitemporal narrowing	+	+	-
Blushy eyebrow	+	+	+
Straight eyebrow	+	+	+
Long eyelashes	+	+	+
Low-set ears	+	+	-
Deep philtrum	+	+	-
Short philtrum	+	+	±
Everted upper lip	+	+	+
Thin upper lip	+	+	+

Prominent upper vermilion	+	+	+
Prominent lower vermilion	+	+	+
Large mouth	-	+	+
Micrognathia/ receding chin	+	+	+
Other	-	-	Pierre Robin sequence
Musculo/skeletal anomalies			
Brachydactyly	-	-	+
Skin/ectodermal features			
Generalized hypertrichosis	+	+	+
Thick hair	+	+	+
Gingival overgrowth	+	+	+
Nail dysplasia	-	-	-

[1]The subject did not reach any milestone at the age of the last evaluation.

[2]Major developmental milestones were achieved within proper age (head control: 3 months, sitting: 7 months, walking: 12 months, single words: 18 months).

[3]Major developmental milestones were delayed (head control: 5 months, crawling: 1 year, walking: around 3 years; single words: 8 years).

1 **Figure Titles and Legends**

2

3 **Figure 1. Clinical features of individuals with *de novo KCNK4* mutations.** (**A-C**) Subject

4 1 (11 months). Note the hypotonic face, bitemporal narrowing, bushy and straight eyebrows,

5 long eyelashes, short deep philtrum, prominent upper and lower vermilion, and receding chin.

6 (**D-F**) Subject 2 at 12 months and 5 years. Evolution of facial appearance is appreciable.

7 Note the bitemporal narrowing, bushy and straight eyebrows, long eyelashes, low-set

8 anteverted ears, short deep philtrum, and prominent upper and lower vermilion. (**G-I**) Subject

9 3 at 8 years. Long eyebrows with mild synophris and long eyelashes, thick hair, large mouth

10 with smooth philtrum, and thin lips can be appreciated. Gingival overgrowth and generalized

11 hypertrichosis occur in all ~~patients~~ affected individuals with different degree of severity.

12

13 **Figure 2. KCNK4 structure and location and structural consequences of disease-**

14 **causing mutations.** (**A**) KCNK4 is a homodimeric channel. The schematic structure of the

15 monomer is shown with the cytoplasmic side pointing down (left panel). Each subunit

16 comprises an extracellular cap covering the pore, four transmembrane helices, M1 to M4,

17 and two pore domains, P1 and P2, constituting the selectivity filter. K^+ ions are shown as

18 white spheres. Locations of mutated residues are highlighted by pink spheres. The

19 crystallographic structure of the KCNK4 dimer (PDB code 4WFF) is also shown (lateral view,

20 middle panel; as seen from the cytoplasm, right panel). One monomer is colored with the

21 same code of the scheme, while the other monomer is reported in gray. (**B**) Structure of the

22 KCNK4 channel in the two conformational states with open and closed lateral fenestrations

23 (PDB codes 4WFF and 4WFE, left and right panels, respectively). Only helix M4 and residue

24 Ala^{244} are highlighted in dark red and pink, respectively. ~~Potassium~~ K^+ ions are shown as

25 white spheres, while the decane molecule inserted in the lateral intramembrane fenestration

26 and blocking the channel is shown as blue spheres. The protein is reported in both ribbon

and surface representations, to illustrate the open and closed states of the fenestration that

allow or avoid the entrance of the aliphatic molecule. (**C**) Structural impact of the p.Ala244Pro

and p.Ala172Glu amino acid substitutions, as observed in the molecular dynamics (MD)

simulations. Histograms of the pore radius of the two lateral openings, observed in the MD

simulations (p.Ala244Pro [green], p.Ala172Glu [orange] and WT [red]) (left panel). The

vertical dashed line indicates the radius of a methane molecule (~2.0 Å). Lateral opening in

the conformation that best represents those observed in the MD simulations are also shown

(right panel). The fenestration is viewed from the lipid-exposed external surface and helices

M4 and M2 are shown in transparency. Residues Leu^{125}, Phe^{246} and Leu^{250}, involved in the

hydrophobic cluster occluding the fenestration are shown in balls and sticks representation.

Figure 3. Whole-cell current recordings from CHO cells expressing wild-type or mutant

KCNK4 channels. (**A**) Representative current recordings elicited with the indicated pulse

protocol consisting of 100-ms voltage steps to potentials between -110 and 100 mV in cells

expressing the wild-type (WT) or mutant (p.Ala244Pro or p.Ala172Glu) KCNK4 channels. (**B**)

The I/V-plot shows means ± SEM of current amplitudes recorded with the voltage step

protocol. Number of experiments is given in parenthesis. Cell transfections were performed

using a 1:10 predilution of *KCNK4* cDNA (final concentration 400 ng/ml). (**C**) I/V-plots of

representative KCNK4 current recordings elicited with shown the ramp protocol shown as

(inset). Cells were previously transfected or co-transfected with cDNA coding for WT and

mutant *KCNK4* cDNA using a predilution of 1:50 for each channel cDNA (final concentration

80 ng/ml and for co-transfection, a total of 160 ng/ml). (**D**) Means ± SEM of the current

amplitude at 0 mV ramp potential. One-way ANOVA with *post-hoc* Bonferroni *t* testing yielded

significant (** p< 0.01, *** p< 0.001) differences compared to WT data. A more detailed

analysis of the whole-cell coexpression experiments is shown in Figure S5.

Figure 4. Current recordings in the outside-out patch-clamp configuration from CHO cells expressing wild-type or mutant KCNK4 channels. (**A**) Overlay of I/V plots of membrane currents repeatedly elicited by the illustrated ramp protocol with intermittent application of positive pressure. Data of a representative experiment on a cell expressing wild-type (WT) KCNK4 (both left panels) and data of experiments with p.Ala244Pro ~~(A244P)~~ or p.Ala172Glu ~~(A172E)~~ KCNK4 channels (right panels). (**B**) Time course of current amplitudes measured at 0 mV ramp potential with intermittent mechanical stimulation; data correspond to the three experiments shown in (A). The filled symbols indicate the illustrated I/V traces. Please note the logarithmic scale used to visualize the time- and pressure-dependent changes. (**C**) Analysis of current recordings directly after the establishment of the outside-out configuration. Box plot of the current amplitudes at 0 mV ramp potential. Data from experiments with cDNA predilution 1:10 for WT KCNK4 (n=10) and the p.Ala244Pro (n=11) and p.Ala172Glu (n=15) KCNK4 mutants. (**D**) Analysis of maximal time- and pressure-induced changes in KCNK4 current amplitudes. Combined data from experiments using 1:10 or 1:50 cDNA predilution for transfection (WT KCNK4, n=16; p.Ala244Pro, n=13; p.Ala172Glu, n=19). Fold current increase was calculated for each experiment as ratio of the maximal (with pressure) to the initial (without pressure) current amplitude at 0 mV. Please note the logarithmic scale of this parameter. Statistical analysis (C and D): Kruskal-Wallis tests yielded significant differences between groups (ANOVA on ranks: p<0.001); *post-hoc* Dunn`s testing yielded significant differences compared to WT data; significance levels were determined with the Wilcoxon-Mann-Whitney test (***, p< 0.001). A more detailed analysis of the outside-out experiments is shown in Figure S6.

Figure 5. The basally activated p.Ala244Pro and p.Ala172Glu KCNK4 mutants do not further respond to arachidonic acid (AA) stimulation. (**A-C**) I/V-plots of current traces

recorded in the whole-cell configuration with a ramp protocol (inset in **A**) from cells previously transfected with cDNA coding for wild-type (WT) KCNK4 (**A**; cDNA predilution 1:10), and p.Ala244Pro (**B**) or p.Ala172Glu (**C**) KCNK4 (each mutant: cDNA predilution 1:50). Control current traces (just before application of AA) and traces illustrating maximal current amplitudes after application of 20 µM AA are superimposed. (**D**) Analysis of AA-induced changes. Please note the logarithmic scale. Application of 20 µM AA resulted in a slowly developing, impressive activation of WT KCNK4 channels (maximal current amplitude at 0 mV in the time period 2-20 min after AA application relative to the value just before AA application is given as fold current increase; median = 66.7). Both mutant channels showed a significantly impaired response to AA (p.Ala244Pro, fold current increase: median = 1.12; p.Ala172Glu, fold current increase: median = 1.06). Asterisks denote significant differences compared to WT data (ANOVA on ranks and *post hoc* Dunn's testing; (*** $p < 0.001$).

Figure 1

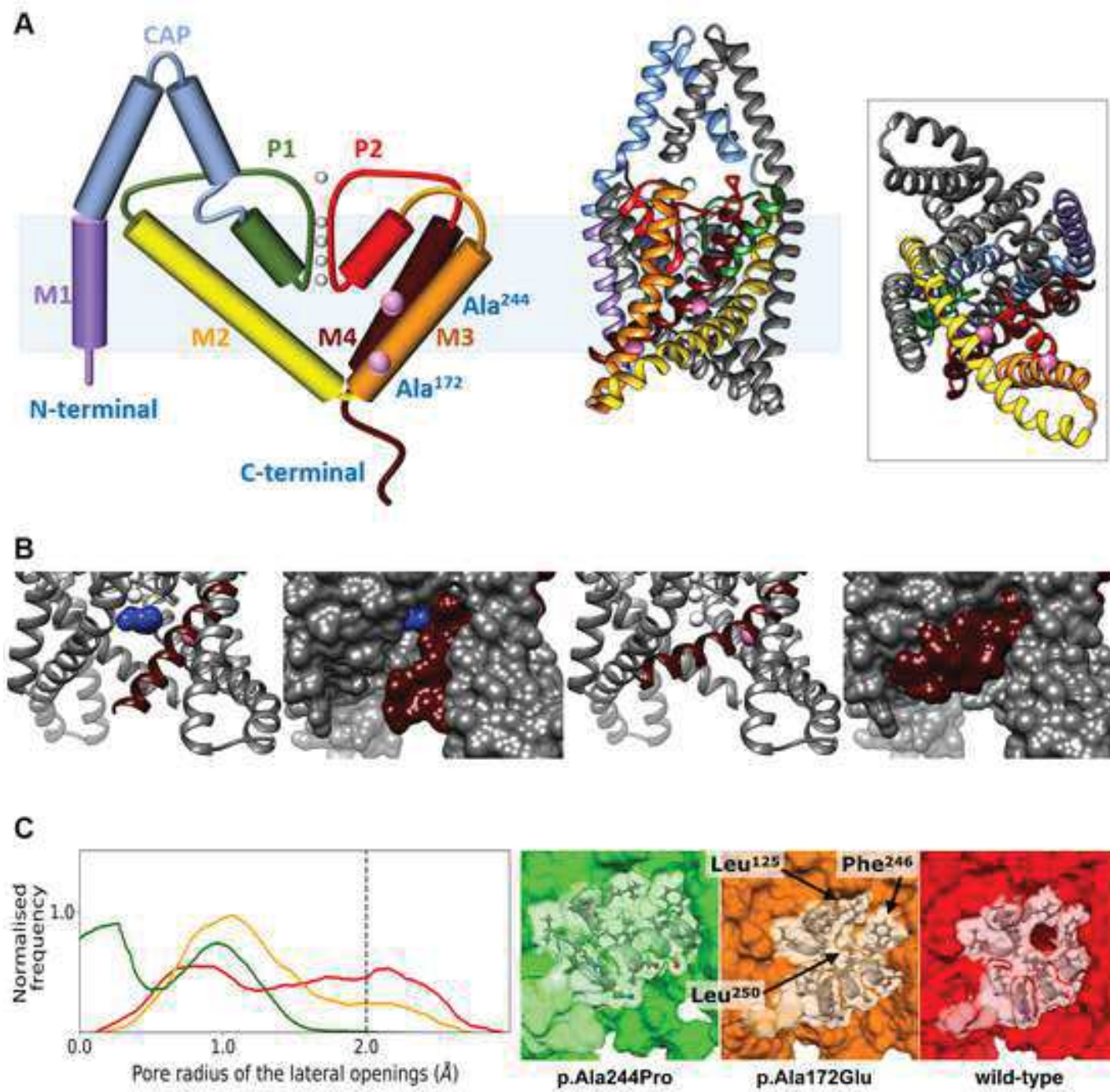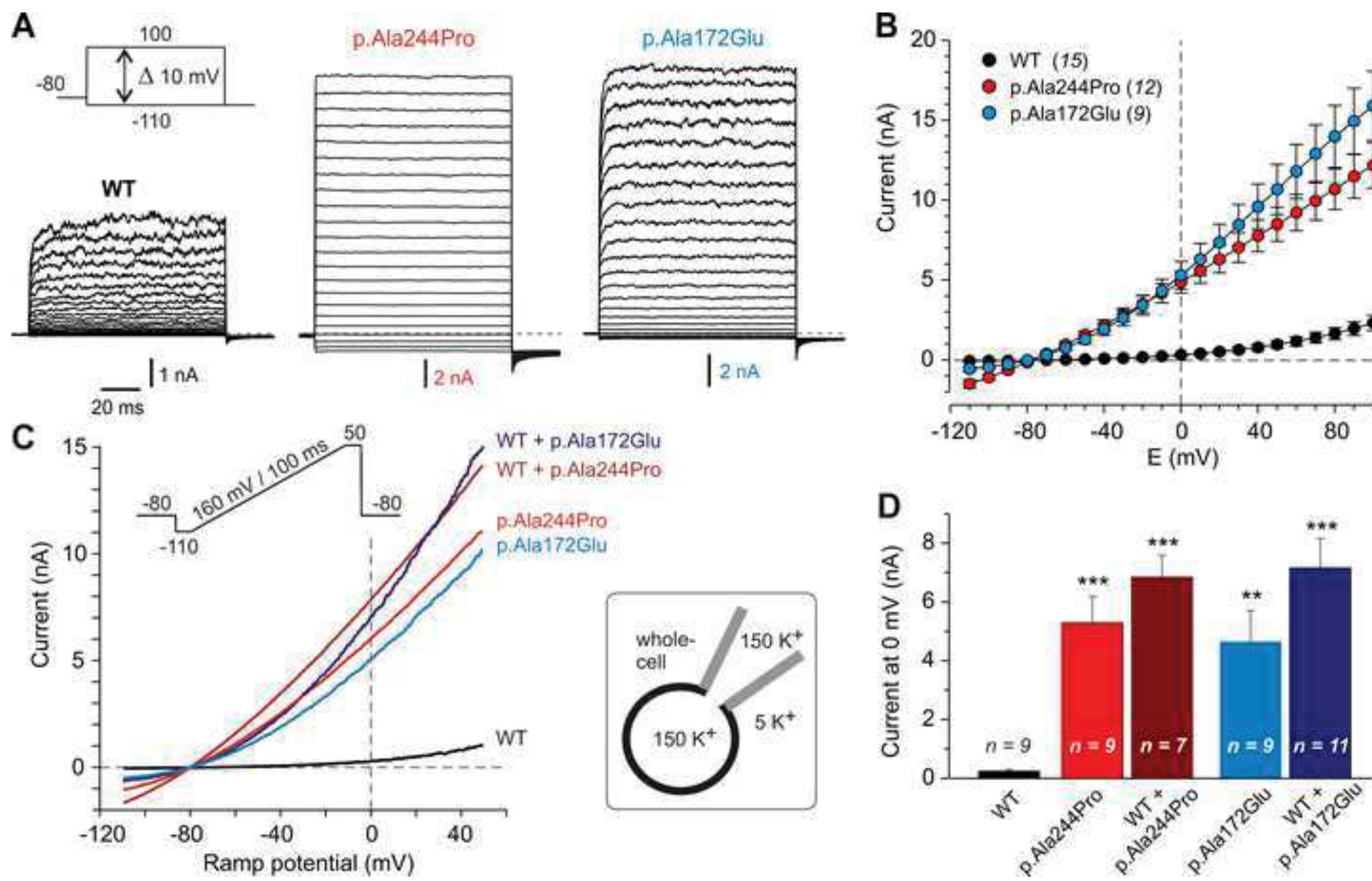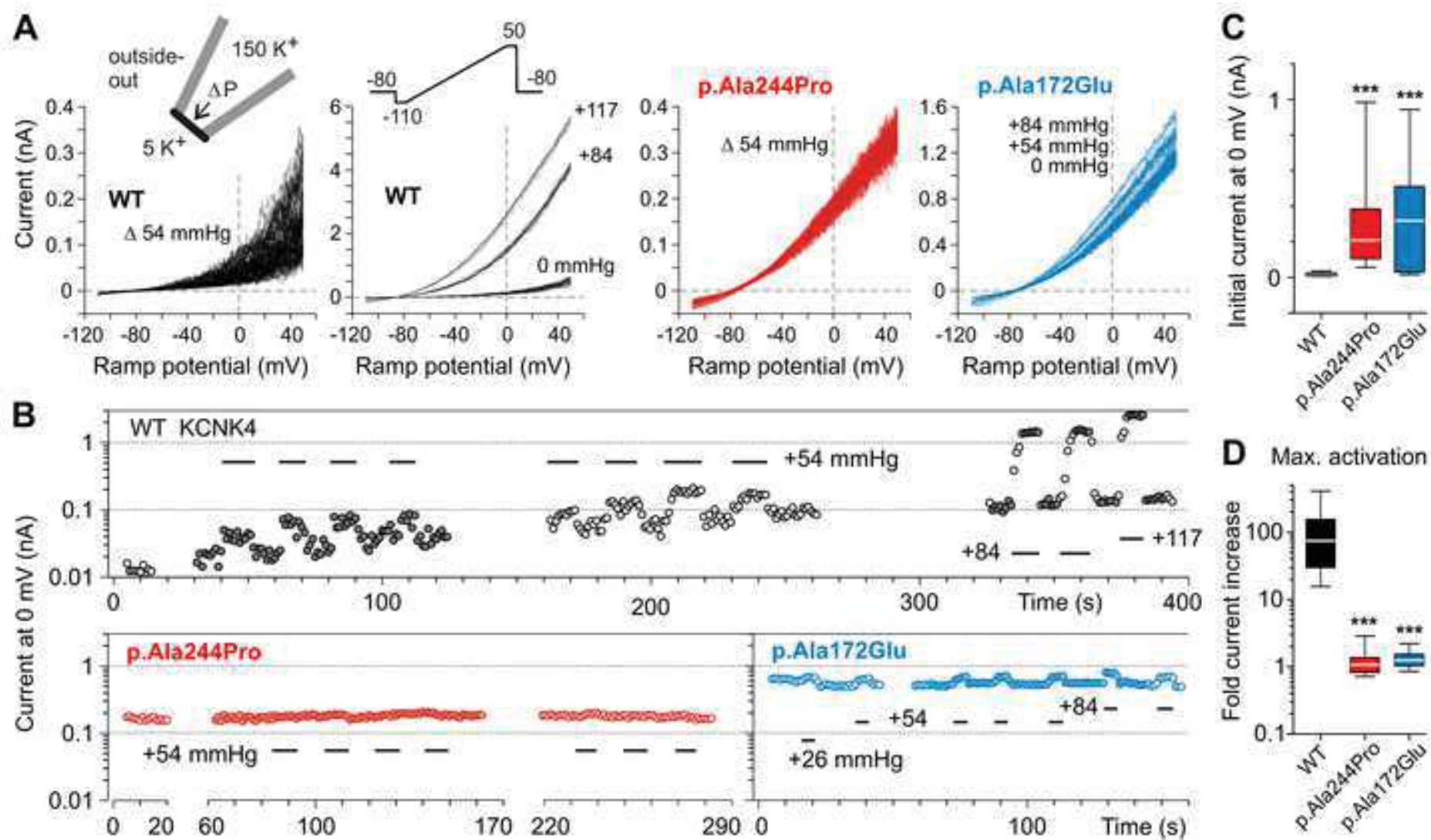Subject 1 c.515C>A (p.Ala172Glu)

Subject 2 c.730G>C (p.Ala244Pro)
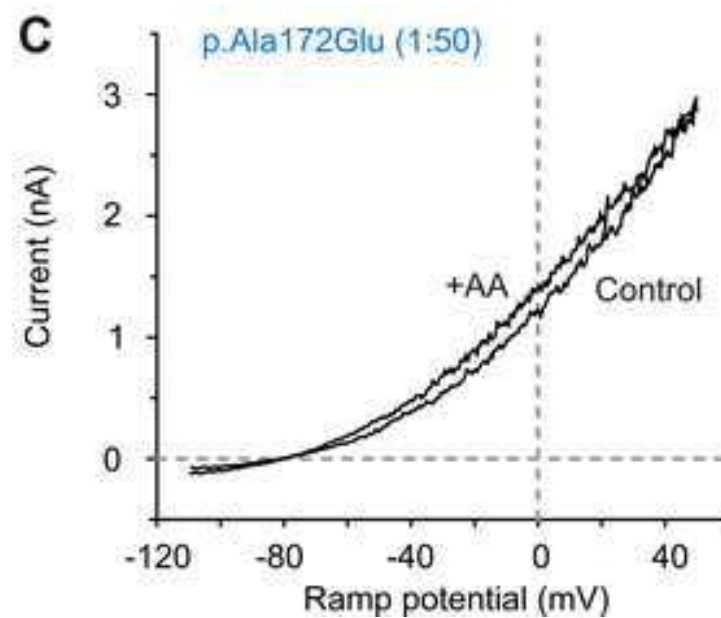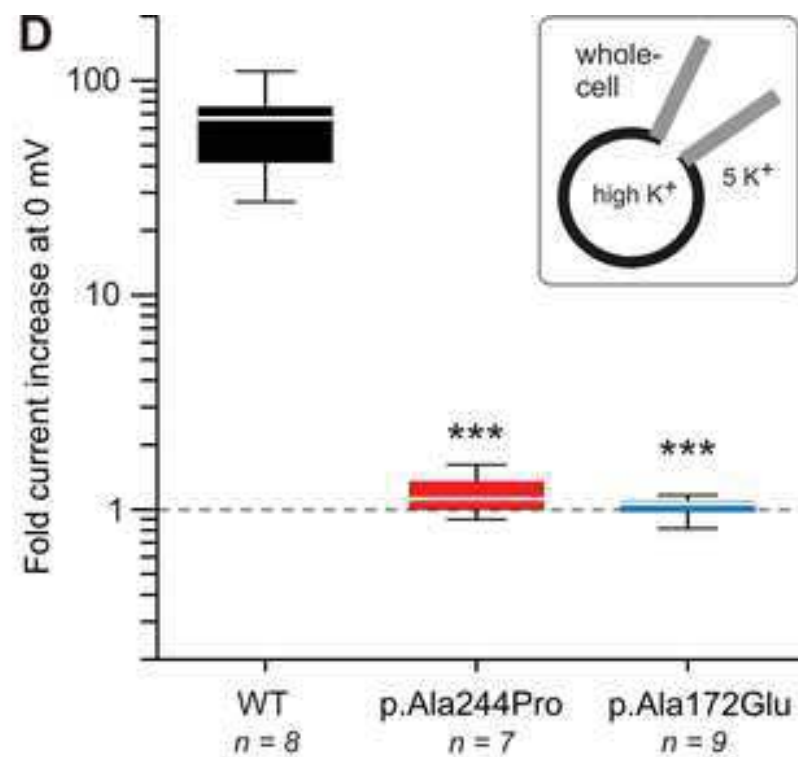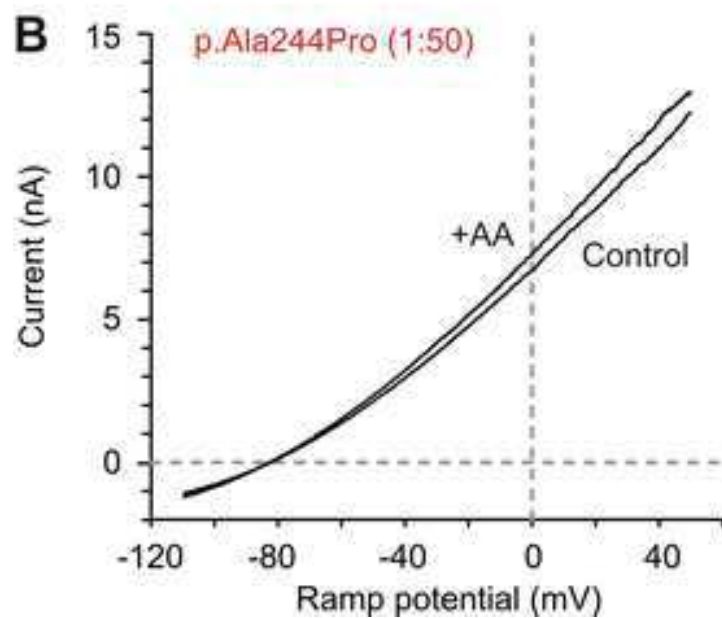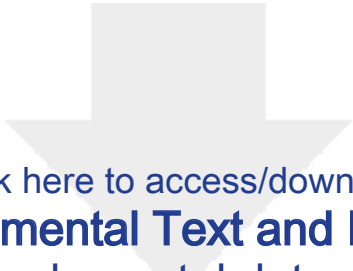
Subject 3 c.515C>A (p.Ala172Glu)

Figure 2

Figure 3

Click here to access/download;Figure;Figure 3.TIF ⬆

Figure 4

Click here to access/download;Figure;Figure 4.tif ⬇

Figure 5

Click here to access/download;Figure;Figure 5.tif
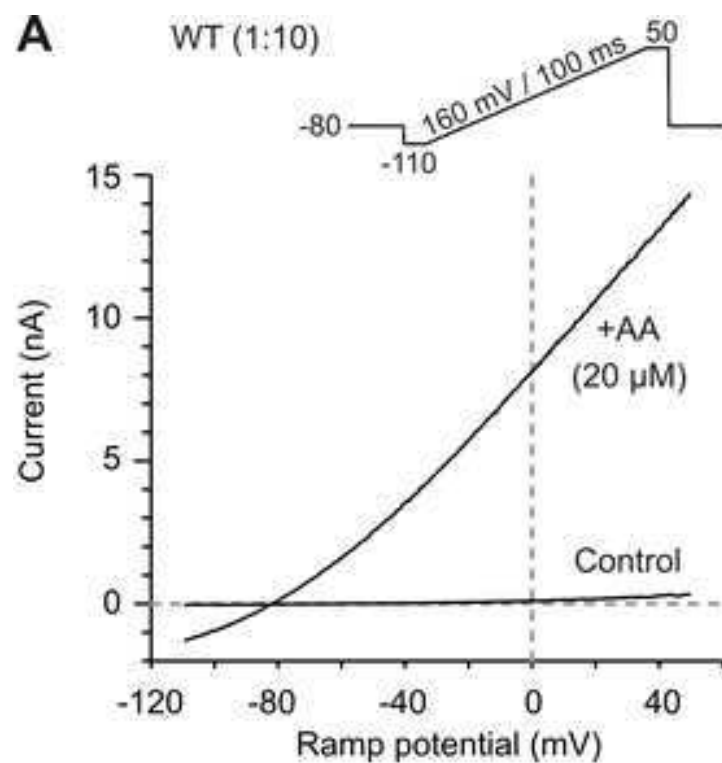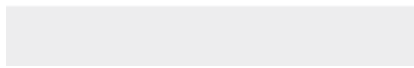
Click here to access/download
Supplemental Text and Figures
supplemental data.pdf

Bambino Gesù
OSPEDALE PEDIATRICO

Autorizzazione all'acquisizione di immagini fotografiche

Data ....22/08/2016....

Cognome ....IUCCI.... Nome ....MASSIMO....

Data di Nascita ....07/09/1973....

Con la presente autorizzo l'acquisizione delle immagini fotografiche di:

( ) me stesso

(X) mio figlio/a ....IUCCI GIACOMO.... Nato/a il ....01/02/2016....

( ) altri miei familiari

E il seguente uso delle immagini fotografiche acquisite:

(X) conservazione nell'Archivio immagini dell'Ospedale Pediatrico Bambino Gesù come materiale sensibile di ausilio diagnostico.

(X) condivisione con altri professionisti per approfondimento diagnostico.

(X) condivisione con altri professionisti per finalità didattiche e di ricerca, compresa l'eventuale pubblicazione in forma anonimizzata.

Il paziente o chi ne fa le veci ....Mariano Iucci....

Il medico che ha raccolto il consenso ....[firma]....

Il tipo di autorizzazione rilasciata non modifica in alcun modo l'impegno che l'Istituto dedicherà alla soluzione del quesito posto in sede di Consulenza Genetica. Il consenso rilasciato può essere modificato in ogni momento.

Bambino Gesù
OSPEDALE PEDIATRICO

Autorizzazione all'acquisizione di immagini fotografiche

Data .....03/03/2016.....

Cognome ....FELICE.......... Nome ....FEDERICA..........

Data di Nascita ....06/06/81..........

Con la presente autorizzo l'acquisizione delle immagini fotografiche di:

( ) me stesso

(X) mio figlio/a ....DISCENZA BIAGIO.......... D.D.N... 22-8-2012

( ) altri miei familiari

E il seguente uso delle immagini fotografiche acquisite:

(X) conservazione nell'Archivio immagini dell'Ospedale Pediatrico Bambino Gesù come materiale sensibile di ausilio diagnostico.

(X) condivisione con altri professionisti per approfondimento diagnostico.

(X) condivisione con altri professionisti per finalità didattiche e di ricerca, compresa l'eventuale pubblicazione in forma anonimizzata.

Il paziente o chi ne fa le veci ....

Il medico che ha raccolto il consenso ....
Dott.ssa Maria Lisa Dentici
Genetica Medica

Il tipo di autorizzazione rilasciata non modifica in alcun modo l'impegno che l'Istituto dedicherà alla soluzione del quesito posto in sede di Consulenza Genetica. Il consenso rilasciato può essere modificato in ogni momento.

Bambino Gesù
Ospedale Pediatrico
Istituto di Ricovero e Cura
a Carattere Scientifico
www.ospedalebambinogesu.it

Joint Commission
International

RESEARCH SUBJECT INFORMATION AND CONSENT FORM

TITLE:	Research to Expand the Understanding of Genetic Variants: Clinical and Genetic Correlations
PROTOCOL NO.:	GeneDx0003 WIRB® Protocol #20171030
SPONSOR:	GeneDx, Inc.
INVESTIGATOR:	Gabriele Richard, MD, FACMG 205 Perry Parkway Gaithersburg, Maryland 20877 USA
STUDY-RELATED PHONE NUMBER(S):	GeneDx, Inc. 301-519-2100 Kirsty McWalter (Study Coordinator) 301-519-2100 x6435

A person who takes part in a research study is called a research or study subject. In this consent form, "you" always refers to the research subject. If you are a parent or guardian of minor, please remember that "you" means the research (study) subject.

SUMMARY

You are being asked to be in a research study. The purpose of this consent form is to help you decide if you want to be in the research study. You should not join this research study until all of your questions are answered. You will receive a copy of this form.

Things to know before deciding to take part in a research study:
- The main goal of a research study is to learn things to help patients in the future.
- The main goal of regular medical care is to help each patient.
- Your decision to join or not join the research study will not cause you to lose any medical benefits. If you decide not to take part in this study, your doctor will still treat you.
- Parts of this study will involve collecting information about standard medical care. Standard care is the care normally given for a certain condition or illness.
- Your medical records may become part of the research record. Your medical records may be looked at and/or copied by GeneDx or other groups associated with the study.
- Your medical insurance may be billed for standard medical care you get during the study. If your insurance company is billed then it may have access to the research records.
- Insurance companies may not pay for treatment that is part of a research study. Taking part in a research study could affect your current or future insurance coverage. In the rare instance that a test or procedure is not considered standard medical care, GeneDx will cover costs on a case-by-case basis.

PURPOSE OF THE STUDY

This research is being done to learn more about genetic changes (variants) and if they cause certain disorders or clinical features. This research is considered experimental. It will only be done with your consent.

PROCEDURES

The research includes the following procedures. At the end of this form, you will choose whether to consent to each procedure.

A. Medical Health Information

We will compare your information (e.g., genetic test results, clinical findings, medical history, family history information) to the information of other people who have had genetic testing. We may contact your doctor(s) or you to confirm details or ask for more information.

B. Medical Photograph(s) and/or Video(s)

Your medical photograph(s) and/or video(s), if available, will be used for teaching, presentations, and publications. Identifying information other than the photograph(s), such as your name, will not be used.

C. Additional Tests or Procedures

Sometimes, other tests or procedures can give more information about your genetic test results or clinical features. As part of standard medical care, we might recommend that you have more studies or tests done. Your healthcare provider(s) will order those studies/tests. We will collect information about these studies/tests. Your health insurance can be billed for those studies/tests. Separately, other additional studies/tests might be suggested for research purposes. In those cases, GeneDx will speak with you before the test/procedure about GeneDx's coverage of the cost, on a case-by-case basis.

D. Additional Samples

In some cases, the additional recommended tests may require another sample of blood, skin, muscle, or other tissue. Usually, only one sample type will be requested, most often blood, buccal, or saliva. Other sample types, such as skin or muscle biopsy, will only be requested in a very small number of cases, and only if all other options have been exhausted. Before any tests are ordered, your doctor or the study coordinator will explain the procedure. You can choose not to have the test(s) done.

The following different sample types may apply:

1. Blood sample: A needle will draw blood. A maximum of 10mL (2 teaspoons) of blood will be drawn. This is usually done in a doctor's office, clinic, or laboratory. You will be able to go home after the sample is drawn.

2. Buccal sample: A brush, swab, or collection device will be used to collect tissue (buccal cells) from the inside surfaces of your cheeks. You should not eat or drink for 30 minutes before collecting the sample.

3. Saliva (oral rinse) sample: You will swish liquid in your mouth, then spit the liquid and saliva into a tube. You should not eat or drink for 30 minutes beforehand.

4. Urine sample: This will involve giving a urine sample in a sterile cup.

5. Hair sample: A few individual hairs will be plucked out of the skin. Hair samples used for genetic testing must have the roots attached.

6. Skin biopsy: A local anesthetic will numb a small area of skin. This is often done with a topical anesthesia (like a numbing cream), but may be done with an injection. The skin biopsy will involve a tool, usually a surgical knife (scalpel), or a small punch the size of a pencil eraser. The tool will remove a piece of skin. Stitches might not be needed for a small skin sample. Stitches might be needed for a large sample. This is done as an outpatient procedure at a doctor's office or clinic. You will be able to go home when it is done.

7. Muscle needle biopsy: A muscle biopsy is usually done as an outpatient procedure at a doctor's office, clinic, or hospital. You will be able to go home when it is done.
   - Needle biopsy: a local anesthetic is often used to numb an area of skin. Then a needle and syringe remove a small sample of muscle tissue.

RISKS AND DISCOMFORTS
There are possible risks and discomforts associated with this study:

1) Personal Health Information: If your personal health information is shared in a publication or presentation, there is a risk that someone could identify you based on the unique combination of your clinical signs/symptoms and your genetic test result. This risk is minimal, because we will not share information such as your name, date of birth, or location. If you consent to having your photograph or video published or presented, there is a chance that someone could recognize you.

   We are very concerned with protecting your confidentiality. To protect against these risks, we will use a unique code instead of name, date of birth, or medical record number. We will keep all information in password-secured, encrypted computers and databases. Also, we will only use general descriptions of clinical signs/symptoms; publish/present cases in groups; and not use photographs of identifiable features (e.g., faces, unique tattoos or features) unless pertinent to the case and with your permission.

2) Blood Sample: There is a risk of discomfort, a small risk of bleeding, and a small risk of bruising where the needle enters the skin. There is a very small risk of infection whenever blood is drawn. A small amount of blood will be taken (less than two teaspoons). Donating this amount of blood will not pose a risk to your health. To protect against risks, blood will be drawn by trained technicians using standard sterile techniques.

3) Buccal sample: The brush, swab, or collection device used to collect tissue (buccal cells) from the inside surfaces of your cheeks may cause minor discomfort.

4) Saliva (oral rinse) sample: Swishing liquid in your mouth and spitting the liquid and saliva into a tube may cause minor discomfort.

5) Urine sample: This will not involve any more risk or discomfort than is typically experienced when urinating

6) Hair sample: Since hair samples used for genetic testing must have the roots attached, removal may cause discomfort at the site of the hair root.

7) Skin Biopsy: There are risks of discomfort, pain, infection, bleeding, and bruising at the biopsy site. If local anesthesia is used, there is a low risk of drowsiness, allergic reaction, headache, blurred vision, and continuing numbness or weakness. Rarely, and more commonly associated with high doses and injection, you could have an allergic reaction, seizure, or cardiac arrest. Most people do not have any complications and little discomfort. To protect against risks, skin biopsies will be done and anesthesia given by trained technicians using standard sterile techniques. Symptoms can be treated by your doctor with local antibiotics and/or pain medication.

8) Muscle Biopsy: There are risks of discomfort, pain, infection, bleeding, and bruising at the biopsy site. There is also a small risk of damage to the muscle where the needle enters, but this is rare. If local anesthesia is used, there is a low risk of drowsiness, headache, blurred vision, and continuing numbness or weakness. Rarely, and more commonly associated with high doses and injection, you could have an allergic reaction, seizure, or cardiac arrest. Most people do not have any complications. To protect against these risks, muscle biopsies will be done and anesthesia given by trained technicians using standard sterile techniques. Symptoms can be treated by your doctor with local antibiotics and/or pain medication.

If you are injured or get sick from being in this research, call your doctor immediately. Your insurance will be billed for any treatment. Insurance may not cover injuries or illness due to participation in a research study.

NEW INFORMATION
You will be told about new information that might change your decision to be in this study. You may be asked to sign a new consent form if this happens.

BENEFITS
We cannot promise that you will get medical benefits from being in this study. If you have more tests done as part of this research, the results might give you more information about your condition. The results of this study may help us learn more about certain conditions. This could help people with similar conditions in the future.

PAYMENT FOR PARTICIPATION
You will not receive payment for this research.

COSTS
You or your insurance company may be billed for any regular medical care. You should check with your insurance company to determine which genetic tests will be covered by your insurance. Tests and procedures that are done only for the research will not be billed to you or your insurance company. If those situations, GeneDx will speak with you before the test/procedure about GeneDx's coverage of the cost, on a case-by-case basis.

ALTERNATIVE TREATMENT
This is not a treatment study. Your alternative is not to be in this study.

AUTHORIZATION TO USE AND DISCLOSE INFORMATION FOR RESEARCH PURPOSES

By signing this consent, you give GeneDx permission to use or release your health information for this research. The health information GeneDx may use or disclose includes:

- Laboratory results (e.g., blood work, molecular tests, and other diagnostic tests).
- Medical record (e.g., clinical information, medical procedures, treatments, clinic notes).
- Medical photograph(s) and/or video(s).
- Research record and information relating to the research project protocol.

Your health information may be shared with the principal investigator, sub-investigators, and research team. This may also include research collaborators, research sponsors, and/or Institutional Review Boards (the Western Institutional Review Board® (WIRB®)) or Data Safety and Monitoring Boards.

Your health information will be collected and used to do the research, to study the research results, and to make sure the research was done right. GeneDx may add your research data to databases to help design better research studies in the future and to learn more about disease.

Your health information may be used or released as required by law. It may be shared with a public health authority authorized by law to collect or receive information to prevent or control disease, injury, disability, and conduct public health surveillance, investigations, or interventions.

GeneDx is required by law to protect your health information. Persons who receive your health information may not be required by federal and state privacy laws (such as the Privacy Rule) to protect it. They may share your information with others without your permission, if allowed by laws that govern them.

You do not have to sign this consent. Refusal to sign will not affect your care or health plan coverage, treatment, payment, enrollment, or eligibility for benefits to which you are entitled. If you do not sign, you will not be included in the research. Your participation is voluntary. You may decide not to participate or may leave the study any time without penalty or loss of benefits you are otherwise entitled to.

Stopping Participation

You can change your mind and take back this consent any time. Taking back this consent is effective when your written notice is received by GeneDx at:

GeneDx, Inc.
Attention: Dr. Gabriele Richard, Principal Investigator
207 Perry Parkway
Gaithersburg, MD, 20877

This consent will not expire. Your health information will be kept indefinitely. If you take back this consent, GeneDx will stop collecting your health information for research. GeneDx will be able to use your health information that was already collected. Information already sent to the research project cannot be withdrawn.

If you withdraw consent, your health insurer may have a legal right to contest a claim, if providing consent is a condition required for insurance coverage. Information disclosed in accordance with this agreement may then be further disclosed by the recipient and may no longer be protected by federal or state law.

Your participation in this research may be stopped at any time by GeneDx, without consent, for any reason, including if it is in your best interest, if you do not consent to continue after being told of changes in the research that may affect you, or if the study is completed or closed.

QUESTIONS

Contact Kirsty McWalter, MS, CGC, Study Coordinator at 301-519-2100x6435 or GeneDx, Inc. at 301-519-2100 if you have questions about participation in this study, feel you have had a research-related injury, or have questions, concerns or complaints about the research.

If you have questions about your rights as a research subject or if you have questions, concerns or complaints about the research, you may contact the WIRB. WIRB independently reviews research. WIRB will not be able to answer some study-specific questions. You may contact WIRB if the research staff cannot be reached or you wish to talk to someone other than the research staff.

Western Institutional Review Board® (WIRB®)
1019 39th Avenue SE Suite 120,
Puyallup, Washington 98374-2115
Telephone: 1-800-562-4789 or 360-252-2500
E-mail: Help@wirb.com

Consent and Assent Instructions:

Consent: *Subjects 18 years and older must sign on the subject line below*
For subjects under 18, consent is provided by the parent or legal guardian
Assent: *Is not required for subjects 6 years and younger*
Written assent is required for subjects ages 7 through 17 years using the Assent
section below.

CONSENT for Patient Name: Peyton Vanderburg **Patient DOB:** 12/09/2009

Parent/Legal Guardian's Name: Tina Vanderburg (if patient is a minor)

GeneDx, Inc. requests permission to use your/your child's medical health information, medical photograph(s), video recording(s), and additional samples. The materials will be used without identifying information such as your/your child's name.

The information may be used for the following:
- To help the laboratory in genetic testing, analysis, and interpretation of results,
- For teaching purposes,
- For medical research, medical publications (electronic or printed publications, medical journals or textbooks), and scientific conferences or seminars. I understand that this information may be seen by the general public, and by scientists and medical researchers who use these publications for professional education. I understand it is possible that someone may recognize me, even though no identifying information will be used.

1. Medical Record Information
   ☑ I consent to release my complete health record (including records relating to mental healthcare, communicable diseases, HIV or AIDS, and treatment of alcohol or drug abuse).

   OR

   ☐ I authorize the release of my complete health record with the exception of:
   ☐ Mental health records;
   ☐ Communicable diseases (including HIV and AIDS);
   ☐ Alcohol/drug abuse treatment
   ☐ Other (please specify):_____

2. Medical Photographs/Videos
   ☑ I consent to release medical photographs/videos for this research.

3. Additional Tests or Procedures
   ☑ I consent to release the results of additional tests or procedures for this research.

4. Additional Samples
   ☑ I consent to release additional samples, as indicated previously in this form, for this research

By signing below, I confirm that I have read and understand this authorization form, the form has been explained to me in terms I understand, I had a chance to ask questions, and I voluntarily consent to the use of my health information, photograph(s), video recording(s), and/or additional samples as outlined above:

_____ (Patient 18 and older Signature) _____ (Date)

Jne Vanderbuy (Parent/Legal Guardian's Signature) 2|04|18 (Date)

Nadia Falah, MD (Person obtaining consent) 02/06/2018 (Date)

_____ (Witness) _____ (Date)

For individuals ages 7 to 17: My signature below indicates that the information in this form has been explained to me in terms I understand, I had a chance to ask questions, and I voluntarily assent to the use of my health information, photographs(s), video recording(s), and/or additional samples as outlined above:

_____ (Patient Signature, if able) _____ (Date)

_____ (Person obtaining assent) _____ (Date)

_____ (Witness) _____ (Date)

02/26/2018 4:11PM (GMT-05:00)
02/26/2018 4:11PM (GMT-05:00)

SUPPLEMENTAL DATA

- **Online methods.**

- **Supplemental Note: Case Reports.**

- **Table S1.** WES data output.

- **Table S2.** List of the rare/private (gnomAD frequency < 0.1%, population-matched in-house DB frequency <2%) variants predicted to have functional impact (CADD score > 15) and affecting known disease-associated genes identified by WES in subjects 1 and 2.

- **Table S3.** Differential diagnosis of FHEIG syndrome.

- **Figure S1.** Multiple alignments of KCNK4 orthologs and human paralogs of the TRAAK/TREK K2P channel subfamily.

- **Figure S2.** Conformation of helix M4, whose bending regulates the opening of the lateral fenestrations.

- **Figure S3.** The selectivity filter of KCNK4 is not affected by the disease-causing p.Ala244Pro and p.Ala172Glu substitutions.

- **Figure S4.** Structural impact of the p.Ala172Glu substitution.

- **Figure S5.** p.Ala244Pro (A244P) and p.Ala172Glu (A172E) KCNK4 channel mutants increase whole-cell K$^+$ conductance.

- **Figure S6.** p.Ala244Pro (A244P) and p.Ala172Glu (A172E) KCNK4 channel mutants increase basal K$^+$ conductance in unstimulated outside-out patches and show impaired response to mechanical stimulation.

- **Figure S7.** Cell-attached current recordings were performed on CHO cells expressing either wild-type (WT), p.Ala244Pro (A244P) or p.Ala172Glu (A172E) KCNK4 channels.

ONLINE METHODS

Molecular dynamics (MD) simulations. Dynamics of wild-type (WT) and mutated KCNK4 (p.Ala172Glu and p.Ala244Pro) proteins were studied in the presence of potassium ions in the channel pore. The experimental crystallographic data on the WT protein (PDB code 4WFE) was used as starting structure (Brohawn et al. 2014). After positioning of missing residues and introduction of the disease-causing amino acid changes, and energy minimization and simulated annealing (Fiser et al. 2000), implemented in the Modeller 9.18 software (Sali and Blundell 1993), the protein was inserted in a pre-equilibrated bilayer membrane composed by 201 1-palmitoyl,2-oleoyl-sn-glycero-3-phosphocholine (POPC) molecules, using the CHARMM-GUI membrane builder (Lee et al. 2016), and solvated using ~40000 TIP3P water molecules (Jorgensen et al. 1983). The biological ionic strength was reproduced by including K^+ and Cl^- ions at a concentration of about 0.15 M (Joung and Cheatham 2008), slightly unbalanced to neutralize the overall charge. MD simulations were performed on about 97000 atoms using the GROMACS simulation package (Abraham et al. 2015); the CHARMM36 force-field was used for protein and lipid atoms (Huang and MacKerll 2013). Long-range electrostatic interactions were calculated using the particle mesh Ewald method (Darden et al. 1993), and the cut-off distance for the non-bonded interactions was set equal to 12.0 Å. The systems –were relaxed first by doing a minimization with 5000 steepest descent cycles, by keeping fixed protein and bilayer atom positions and leaving water and ions to adjust freely, followed by a seven-step equilibration protocol with progressively weakened position restraints on protein and lipid atoms. The systems were first equilibrated for 50 ps in the NVT ensemble at 303.15 K using the Berendsen thermostat with a relaxation time of 1 ps and then for 325 ps at constant pressure (1 atm) using the Berendsen weak-coupling anisotropic barostat, with a relaxation time of 5 ps. Finally, the systems were simulated at the production temperature and pressure without any positional restraints. This final equilibration dynamics of 50 ns was then followed by 100 ns production dynamics, with the same settings. The SHAKE constraint to all the hydrogen atoms and a 2 fs time-step were used in all the simulations (Ryckaert 1977).

Configurations explored during molecular dynamics simulations were clustered by applying a simple linkage method (Everitt 2011), with a cut-off distance of 1.2 Å. The main structural features of each protein were inferred by the analysis of the representative conformation for the most populated cluster in the corresponding MD simulation. Curvature of M4 helices was calculated by the Bendix algorithm (Dahl et al. 2012). The radius of both the lateral opening

and ion conduction pathway was calculated for each protein configuration in the MD simulations, using the HOLE algorithm (Smart et al. 1996). In the case of lateral fenestrations, the pore radius was defined as the average radius found along the fenestration axis in a range of 1 Å around the position of heavy atoms flanking the opening (C_β of Phe246, $C_{\delta 1}$ and $C_{\delta 2}$ of Leu250 and Leu125). Salt bridge formation was detected by calculating the distance between the centroids of the anionic carboxylate of glutamate and the cationic guanidinium of arginine, calculated as the average position of their heavy atoms.

Electrophysiology. Patch-clamp experiments were performed 1 to maximally 3 days after CHO cell transfection in the conventional whole-cell configuration, the outside-out configuration or the cell-attached configuration of the patch-clamp technique. The external Ringer solution contained 140 mM NaCl, 5 mM KCl, 0.8 mM $MgCl_2$, 1 mM $CaCl_2$, 5 mM glucose and 10 mM HEPES; pH adjusted to 7.4 with NaOH. The "standard" pipette solution contained 140 mM KCl, 2 mM $MgCl_2$, 1 mM $CaCl_2$, 2.5 mM EGTA and 10 mM HEPES; pH adjusted to 7.3 with KOH yielding a final K^+ concentration of about 150 mM. For arachidonic acid (AA) experiments with prolonged whole-cell recordings, the "low chloride" pipette solution contained 130 mM K^+ aspartate, 2.1 mM $MgCl_2$, 8.55 mM $CaCl_2$, 10 mM EGTA and 10 mM HEPES; pH adjusted to 7.2 with KOH yielding a final K^+ concentration of about 160 mM. Patch pipettes had resistances of 2 to 3 MΩ when filled with standard solution. The access resistance in the whole-cell configuration ranged from 2.5 to 5 MΩ. If possible (all most experiments on WT channels), series resistance was compensated for by at least 70%. Data obtained with standard pipette solution were not corrected for the liquid junction potential error of about 4 mV and no leak subtraction was performed. In experiments with low chloride pipette solution, data were online corrected for a liquid junction potential of about -13 mV for an aspartate-based solution. An EPC-9 patch clamp amplifier was used in combination with the PATCHMASTER stimulation and data acquisition software (HEKA Elektronik, Lambrecht, Germany). All experiments were performed at room temperature. In outside-out experiments, positive pressure was manually applied to the interior of the patch pipette via a calibrated syringe system. In the cell-attached configuration, negative pressure was in the range of -20 to -50 mmHg. External solutions containing AA were freshly prepared from frozen stocks and sonicated just before application; the final concentration was 20 µM. 10 mM stocks of AA sodium salt (Sigma/Merck) dissolved in DMSO were stored at -20 °C and used within 3 days. Control application of DMSO alone (final concentration 0.2%) had no effect on KCNK4 current amplitude.

Patch-clamp data processing was performed with FITMASTER (HEKA), Excel (Microsoft Corp.) and Sigmaplot 11.0 (Systat Software). In voltage step experiments, current amplitudes were determined as mean values during the last period of the 100-ms test pulses. Three parameters were determined to characterize whole-cell and outside-out membrane currents recorded with the voltage ramp protocol: 1) current amplitude at 0 mV ramp potential (almost unaffected by unspecific leak current, but underestimating the true K^+ current amplitude due to voltage errors resulting from uncompensated series resistance); 2) conductance at -80 mV (less affected by series resistance errors, but including unspecific leak conductance); 3) reversal potential (close to the resting membrane potential). High K^+ conductance shifts the reversal potential to the K^+ equilibrium potential. A pressure-induced drop in the reversal potential (change to less negative values) indicated reduced seal resistance. Current amplitudes at 0 mV ramp potential were determined as mean value between -4 and +4 mV ramp potential. Conductance at 0 mV was determined as I/V slope between -8 and +8 mV ramp potential. Similarly, conductance at -80 mV was determined as I/V slope between -88 and -72 mV ramp potential. The reversal potential was determined as the ramp potential with the first reversal from inward to outward current. Due to the high amplitude of currents associated with p.Ala244Pro and p.Ala172Glu KCNK4 expression, relatively fast (100-ms) voltage ramps were used to limit effects of local K^+ concentration changes.

Statistical testing was performed with Sigmaplot 11.0. Experimental data of whole-cell experiments and values of the reversal potential in outside-out experiments are presented as means ± SEM, with *n* representing the number of experiments from different cells. In these experiments, one way ANOVA with *post hoc* Bonferroni *t*-test was used to test for significance as indicated with $\alpha = 0.05$. The effect of pressure stimulation on the reversal potential was analyzed with Student´s two-tailed paired *t* test. Current and conductance values in outside-out and cell-attached patch experiments showed high variability possibly due to channel clustering. These data are presented as box plot (Cleveland method; boxes indicate the 25 to 75% range, whiskers the 10/90 percentiles and points indicate the 5/95 percentiles; the median is shown as line). Statistical analyses were performed with nonparametric ANOVA on ranks (Kruskal-Wallis test) with *post hoc* Dunn's test to identify the significantly differing groups. If significant differences were found between channel mutants and WT data, the individual significance level was determined with the Wilcoxon-Mann-Whitney test. The effect of pressure stimulation (paired data) was analyzed with the Wilcoxon signed rank test.

References

Abraham, M.J., Murtola, T., Schulz, R., Páll, S., Smith, J.C., Hess, B., and Lindahl, E. (2015). GROMACS: High performance molecular simulations through multi-level parallelism from laptops to supercomputers. SoftwareX 1-2, 19-25.

Brohawn, S.G., Campbell, E.B., and MacKinnon, R. (2014). Physical mechanism for gating and mechanosensitivity of the human TRAAK K+ channel. Nature 516, 126-130.

Darden, T., York, D., & Pedersen, L. (1993). Particle mesh Ewald: An N· log (N) method for Ewald sums in large systems. *The Journal of chemical physics*, *98*(12), 10089-10092.

Everitt, B.S., Landau, S, Leese, M., and Stahl, D. (2011). Cluster Analysis. 5th edition (Wiley Series in Probability and Statistics, Wiley).

Fiser, A., Do, R.K.G., and Šali, A. (2000). Modeling of loops in protein structures. Protein Sci. 9, 1753-1773.

Huang, J., and MacKerell, A.D. (2013). CHARMM36 all-atom additive protein force field: Validation based on comparison to NMR data. J. Computat. Chem. 34, 2135-2145.

Jorgensen, W. L., Chandrasekhar, J., Madura, J. D., Impey, R. W., & Klein, M. L. (1983). Comparison of simple potential functions for simulating liquid water. *The Journal of chemical physics*, *79*(2), 926-935.

Joung, I.S., and Cheatham T.E. III. (2008). Determination of Alkali and Halide Monovalent Ion Parameters for Use in Explicitly Solvated Biomolecular Simulations. J. Phys. Chem. 112, 9020-9041.

Lee, J., Cheng, X., Swails, J.M., Yeom, M.S., Eastman, P.K., Lemkul, J.A., Wei, S., Buckner, J., Jeong, J.C., Qi, Y, et al. (2016). CHARMM-GUI Input Generator for NAMD, GROMACS, AMBER, OpenMM, and CHARMM/OpenMM Simulations Using the CHARMM36 Additive Force Field. J. Chem. Theor. Comp. 12, 405-413.

Ryckaert, J.-P., Ciccotti, G., and Berendsen, H.J.C. (1977). Numerical Integration of the Cartesian Equations of Motion of a System with Constraints: Molecular Dynamics of n-Alkanes. J. Comp. Phys. 23, 327-341.

Šali, A., and Blundell, T.L. (1993). Comparative Protein Modelling by Satisfaction of Spatial Restraints. J. Mol. Biol. 234, 779-815.

SUPPLEMENTAL NOTE: CASE REPORTS

Subject 1

The proband, a male, is the second child of healthy non-consanguineous Italian parents. Family history was unremarkable. He was born at term of an uneventful pregnancy. Birth weight was 3,925 g (50th-75th centile), length 54 cm (75th-90th centile) and OFC 34 cm (50th-75th centile). Apgar scores were not available. No perinatal complication are reported. Due to bronchiolitis, hospital admission at 13th day of life revealed nystagmus with absence of visual contact, papillary pallor (FOO) and visual impairment based on visual evoked potentials. Motor developmental milestones were significantly delayed.

At 11 months, brain MRI showed thin corpus callosum and VVLL enlargement. Audiological examination by pure tone audiometry, abdominal ultrasound and echocardiogram were normal. No seizure had been reported. However, first EEG analysis revealed a disorganized pattern characterized by medium-voltage asymmetric theta activity increasing in amplitude and intermingled with spikes over the right temporal areas. Low-voltage fast activity over the frontal regions was recorded in sleep followed by abundant high-voltage theta activity (frontal and centrotemporal areas). No physiological non-REM activity was registered. A subsequent EEG control disclosed a disorganized pattern with diffuse slow waves activity without any epileptic discharge. Biochemical and metabolic screening including serum total testosterone, dihydrotestosterone, 17-OH progesterone, DHEA, cortisol, urine determination of glycosaminoglycans (GAG) and screening for inborn errors of amino acid metabolism were normal.

Clinical evaluation at 11 months disclosed hypotonic face, bitemporal narrowing, bushy and straight eyebrows, long eyelashes, deep-set eyes, low-set ears, short deep philtrum, prominent upper and lower vermilion, mild gingival overgrowth and generalized hypertrichosis (Figure 1).

Postnatal genetic analyses including array-CGH, genes related to Cornelia de Lange and Coffin-Siris syndromes, and clinical exome sequencing were negative.

Subject 2

The proband is the only male child of non-consanguineous Italian parents with unremarkable family history. Pregnancy was uneventful and delivery at term. Birth weight was 3,030 g (25th-50th centile), length 49 cm (25th-50th centile), and OFC 34 cm (50th-75th centile). Apgar scores were 9-10 at 1 and 5 min. At birth, generalized hypertrichosis was evident and

routine laboratory investigations (including serum total testosterone, dihydrotestosterone, 17-OH progesterone, DHEA) and adrenal ultrasound were performed and resulted normal. At 10 months of age, he presented focal clonic seizures in the right side of the body with secondary generalization and diffuse hypertonia, lasting few minutes, with a frequency of two episodes per day. Ictal EEGs showed epileptic discharges from left parietal-temporal and occipital regions with rapid diffusion, while interictal EEGs showed a good differentiation of background cerebral activity without epileptic discharges. At this age, the motor and cognitive development was slightly delayed as demonstrated by the Griffiths Developmental Scale, showing a general quotient of 85, with an impairment in the language and manual coordination areas. Brain MRI showed mild enlargement of bilateral frontal-insular and temporal subarachnoid spaces, but no gross cerebral malformations were evident. He initially started treatment with levetiracetam with transitory control of seizures, then he switched to carbamazepine with full control of seizure occurrence. Therefore, pharmacological treatment was gradually decreased until the drug was suspended at 2 years and 6 months of age. After one month from suspension, seizures occurred and carbamazepine was again introduced efficaciously. Abdominal ultrasound and echocardiogram were normal. Skeletal X-ray survey and metabolic screening including urine determination of glycosaminoglycans (GAG) and screening for inborn errors of amino acid metabolism were normal. ~~Gross g~~Gingival hypertrophy was evident before any anti-epileptic treatment, and ~~became~~ progressively ~~evident~~ worsened (Figure 1), until surgical treatment was required at 5 years and 6/12 because of functional difficulty in chewing and talking.

At the last evaluation, at 5 years and 7 months, auxological parameters were within normal range (height 104 cm, 50th centile; weight 15.5 kg, 10th centile; OFC 51.2 cm, 25th centile). Clinical evaluation revealed generalized hypertrichosis, bitemporal narrowing, bushy and straight eyebrows, long eyelashes, low-set anteverted ears, short deep philtrum, prominent upper and lower vermilion, progressive gingival fibromatosis (surgically corrected before the last evaluation), deep palmar creases and 5th fingers clinodactyly.

He was seizure-free on carbamazepine treatment. At last evaluation, the Developmental Profile 3 (DP-3) score showed a general developmental index of 85 (in details, physical: 83; adaptive behavior: 111; social-emotional: 93; cognitive: 70; communication: 85), confirming a borderline ~~developmental~~ cognitive profile.

Genetic analyses, including peripheral blood karyotype and mutation scan of the coding sequence of *ABCC9*, *ARID1A*, *ARID1B*, *SMARCE1*, *SMARCA4*, *SMARCB1* and *SOX11*

genes, were negative for pathogenic lesions. Array-CGH (44K; Agilent) disclosed a 3p14.2 deletion of 290 Kb (58,790,705-59,080,837) inherited from the mother.

Subject 3

The subject, an 8 year-old female, is the first child of healthy non-consanguineous parents of European descent. Family history was unremarkable, and she has three healthy siblings. She was born at term of an uneventful pregnancy. Birth weight was 3,580 g (50th-75th centile), and length 52.07 cm (75th centile). Her OFC at birth is not available. APGARs reported low, and the patient required resuscitation mainly due to the Pierre Robin sequence and the cleft palate, which were managed clinically and corrected surgically at 10 months of age. Later, before the end of the second year, she developed a seizure disorder, which currently is severe generalized, consisting of tonic-clonic and absence seizures responsive to a high dose of antiepileptic medications: levetiracetam, oxcarbamazepine, carbamazepine, clonazepam, and pyridoxine.

All her milestones were moderately to severely delayed: she started head support at 5 months, crawling at 1 year, and walking at around 3 years. She currently says a few words (e.g., "mama", "dada", "baba"", hut oh", and "no"), but she doesn't understand the meaning behind these words. On examination, the proband has distinctive facial features, which were observed since birth, consistent of bushy and thick eyebrows with synophrys, long eyelashes, micrognathia, gingival hyperplasia, large mouth with a smooth philtrum and thin everted upper lip (Figure 1). She has a generalized hypertrichosis and thick hair. She has nystagmus, and her eye exam revealed an optic hypoplasia. Her growth parameters are within the normal range (height 124.4 cm, 25th-50th centile; weight 22.6 kg, 10th-25th centile; OFC 52 cm, 25th centile). Her skeletal finding are significant for upper and lower extremity brachydactyly and congenital hip dysplasia surgically corrected at 8 years of age.

First genetic assessment, including chromosomal microarray and fragile X analysis, was uninformative.

Table S1. WES data output.

ID	WES enrichment kit	Sequencing platform	Target regions covered >10x	Target regions covered >20x	Average depth on target
Subject 1	SureSelect ClinicalExome V.2 (Agilent)	NexSeq500	91.9%	83.7%	77x
Subject 2	Nextera V.1.2 (Illumina)	HiSeq2000	94.5%	89.2%	76x
Subject 3	IDT xGen Exome Research Panel v1.0	HiSeq4000	98.4%	94.75%	85x

	Subject 1	Subject 2	Subject 3
Number of variants with predicted functional effect[1]	13,484	14,574	4,588
Novel, clinically associated, and unknown/low frequency variants	422[2]	390[2]	204[2]
Putative shared candidate genes (AR/X-linked inheritance)		0[3]	0
Putative shared candidate genes (AD inheritance)		1[4]	1[5]

[1]High quality nonsynonymous changes and changes with potential impact on transcript processing.
[2]MAF <0.1% in gnomAD V. 2.0 database and frequency <1% in our *in-house* database.
[3]Shared genes with variants with CADD scaled score <15, excluding those predicted as benign/likely benign by M-CAP algorithms and interVar.
[4]Shared genes with variants with CADD scaled score <15, excluding those predicted as benign/likely benign by M-CAP algorithms and interVar.
KCNK4: subject 1: NM_001317090.1:c.515C>A, p.Ala172Glu (CADD = 33, M-CAP = 0.028; hg19, chr11:64064979); subject 2: NM_001317090.1:c.730G>C, p.Ala244Pro (CADD = 29.5, M-CAP = 0.038; hg19, chr11:64065650).
[5]*KCNK4* (NM_001317090.1:c.515C>A, p.Ala172Glu).

For a list of the rare/private variants predicted to have functional impact and affecting known disease-associated genes in subjects 1 and 2 see Table S2. No variant satisfied these criteria in subject 3.

Table S2. List of the rare/private (gnomAD frequency < 0.1%, population-matched in-house DB frequency <2%) variants predicted to have functional impact (CADD score > 15) and affecting known disease-associated genes identified by WES in subjects 1 and 2.

Gene	Nucleotide change	Predicted amino acid change	Status	Disease	OMIM
Subject 1[a]					
WNK1	c.6649C>T	p.Arg2217Cys	Het.	Pseudohypoaldosteronism 2C (AD)	614492
TOPORS	c.74C>T	p.Ser25Leu	Het.	Retinitis pigmentosa 31 (AD)	609923
TRPA1	c.2987G>A	p.Arg996His	Het.	Episodic pain syndrome, familial, 1 (AD)	615040
TLL1	c.2783G>A	p.Arg928Gln	Het.	Atrial septal defect 6 (AD)	613087
PKD1	c.8473C>T	p.Leu2825Phe	Het.	Polycystic kidney disease 1 (AD)	173900
CACNA1G	c.3221C>T	p.Ser1074Leu	Het.	Spinocerebellar ataxia 42 (AD)	616795
FOXC1	c.92_100delCGGCGGCCG	p.Ala31_Ala33del	Het.	Anterior segment dysgenesis 3 (AD), Axenfeld-Rieger syndrome, type 3 (AD)	601631 602482
APC	c.2438A>T	p.Asn813Ile	Het.	Adenomatous polyposis coli/Gardner syndrome (AD), Desmoid disease, hereditary (AD)	175100 135290
MYO7A	c.4447A>G	p.Ser1483Gly	Het.	Deafness, autosomal dominant 11 (AD), Deafness, autosomal recessive 2 (AR), Usher syndrome, type 1B (AR)	601317 600060 276900
NOTCH2	c.6343A>G	p.Ser2115Gly	Het.	Alagille syndrome 2 (AD), Hajdu-Cheney syndrome (AD)	610205 102500
IHH	c.315+8C>T	.	Het.	Acrocapitofemoral dysplasia (AR), Brachydactyly, type A1 (AD)	607778 112500
Subject 2[b]					
SPTA1	c.6789-9_6789-8dupTT; c.6430G>A	.; p.Glu2144Lys	Comp. het.	Elliptocytosis-2 (AD), Pyropoikilocytosis (AR), Spherocytosis, type 3 (AR)	130600 266140 270970
MID1	c.229G>A	p.Val77Ile	Hem.	Opitz GBBB syndrome 1 (XLR)	300000
WAS	c.623C>T	p.Thr208Met	Hem.	Neutropenia, severe congenital (XLR), Thrombocytopenia, X-linked (XLR), Wiskott-Aldrich syndrome (XLR)	300299 313900 301000

Het., heterozygous; comp. het., compound heterozygosity; Hem., hemizygous.

[a]WES was performed in the proband only.

[b]WES performed using a trio-based approach (affected child and unaffected parents).

Table S3. Differential diagnosis of FHEIG syndrome.

	FHEIG syndrome	Cantú syndrome	Wiedemann-Steiner syndrome	Temple-Baraitser syndrome	Zimmermann-Laband syndrome, type 1	Zimmermann-Laband syndrome, type 2	Coffin-Siris syndrome
Genes	KCNK4	ABCC9, KCNJ8	KMT2A	KCNH1	KCNH1	ATP6V1B2	ARID1B, ARID1A, SMARCB1, SMARCA4, SMARCE1
Inheritance	AD	AD	AD	AD	AD	AD	AD
ID/DD	+	+	+	+	+	+	+
Seizures/EEG anomalies	+	(+)	(+)	+	+	-	(+)
Hypertrichosis	+	+	+	-	(+)	+	+
Coarse face	(+)	+	(+)	(+)	+	+	+
Facial appearence	Bitemporal narrowing, thick hair, blushy and straight eyebrows, long eyelashes, down-slanting palpebral fissures, broad nasal bridge, deep philtrum, large mouth with everted thin upper lip and prominent upper and lower vermilions	Bitemporal narrowing, low anterior hairline, epicanthal folds, broad nasal bridge, long philtrum, large mouth with thin upper lip and prominent upper and lower vermilions, and increased skin wrinkling	Bitemporal narrowing, thick hair, blushy and straight eyebrows, long eyelashes, narrow palpebral fissures, down-slanting palpebral fissures, hypertelorism, deep philtrum with prominent upper vermilion	Bitemporal narrowing, low anterior hairline, thick hair, blushy and straight eyebrows, long eyelashes, hypertelorism, epicanthal folds, broad nasal bridge, long philtrum, large mouth with everted upper lip	Thick hair, blushy and straight eyebrows, long eyelashes, long deep philtrum, large mouth and thin upper lip	Thick hair, straight eyebrows, long eyelashes, up-slanting palpebral fissures, hypertelorism, hypoplastic alae nasi, broad nasal base, "Bifid" nasal tip, deep philtrum, large mouth, prominent upper and lower vermilions	Bitemporal narrowing, low anterior hairline, blushy and straight eyebrows, long eyelashes, broad nasal bridge, upturned nasal tip, thick alae nasi, broad nasal base, deep philtrum, large mouth, thin upper lip and prominent lower vermilion
Gingival overgrowth	+	+	-	(+)	+	+	(+)
Hearing loss	-	-	-	-	(+)	(+)	(+)
Aplastic or hypoplastic nails	-	-	-	Thumb	+	+	+
Aplastic or hypoplastic terminal phalanges	-	(+)	-	Thumb	+	+	+
Scoliosis	-	(+)	-	(+)	+	+	(+)
Distinguishing features	Combination of hypertrichosis, gingival overgrowth, ID, and EEG anomalies/ epilepsy	Combination of hypertrichosis, macrosomia, osteochondro-dysplasia and cardiomegaly	Peculiar pattern of hypertrichosis involving cubiti and dorsum	Broad and proximally implanted thumbs, long great toes	Combination of hypertrichosis, gingival overgrowth, and hypoplasia or aplasia of nails and terminal phalanges	Combination of hypertrichosis, gingival overgrowth and hypoplasia or aplasia of nails and terminal phalanges	5th finger hypoplasia

+, present in a majority of affected individuals; (+), present in a minority of affected individuals; -, absent.
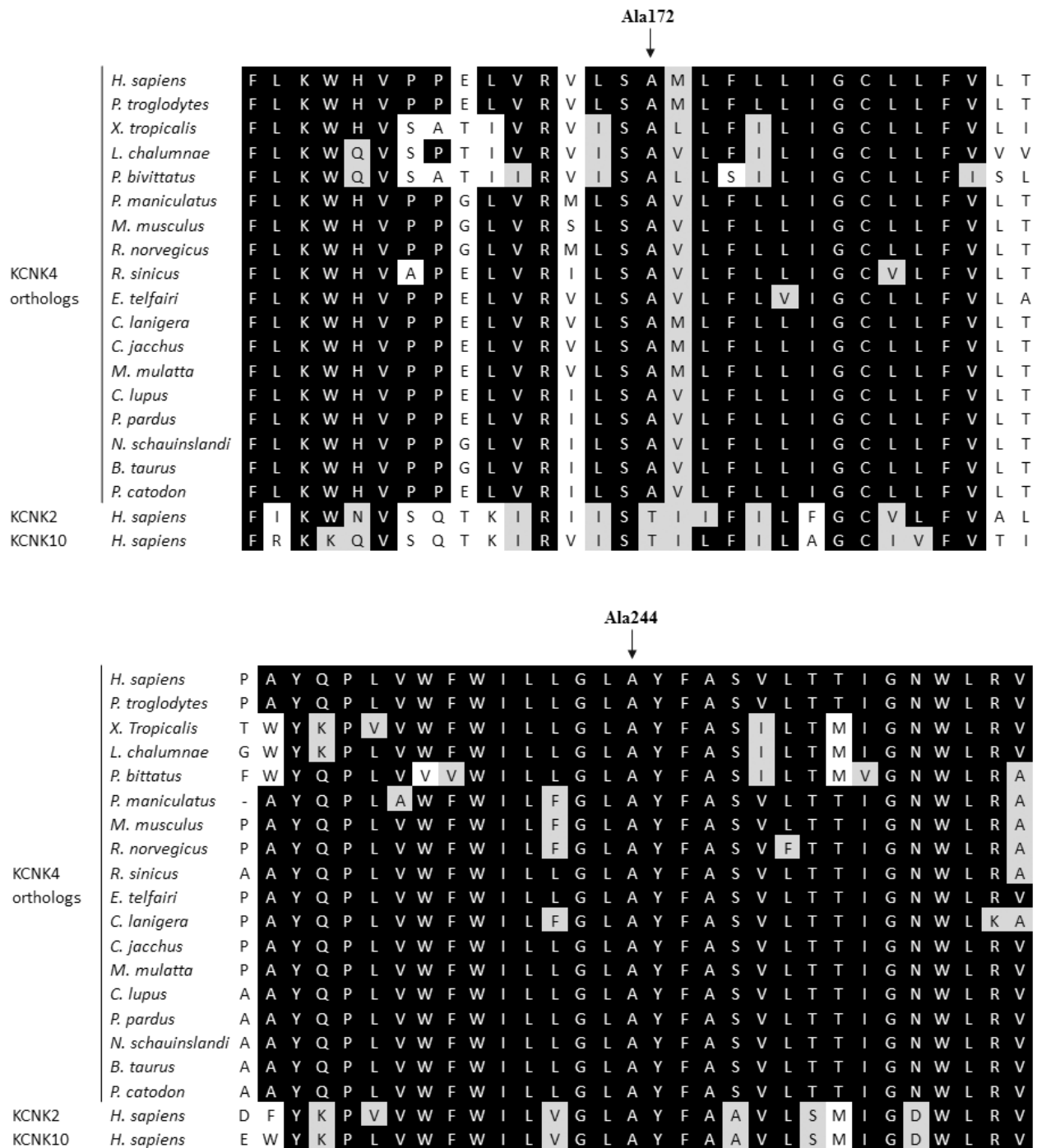
Figure S1. Multiple alignments of KCNK4 orthologs and human paralogs of the TRAAK/TREK K2P channel subfamily. Invariant residues among proteins are highlighted in black. Gray and white background indicate residues with high (> 0.5, Gonnet PAM 250 matrix) and poor (≤ 0.5, Gonnet PAM 250 matrix) degree of conservation, respectively. Alignment was generated using MUSCLE v3.8. KCNK2 and KCNK10 correspond to TREK-1 and TREK-2, respectively.
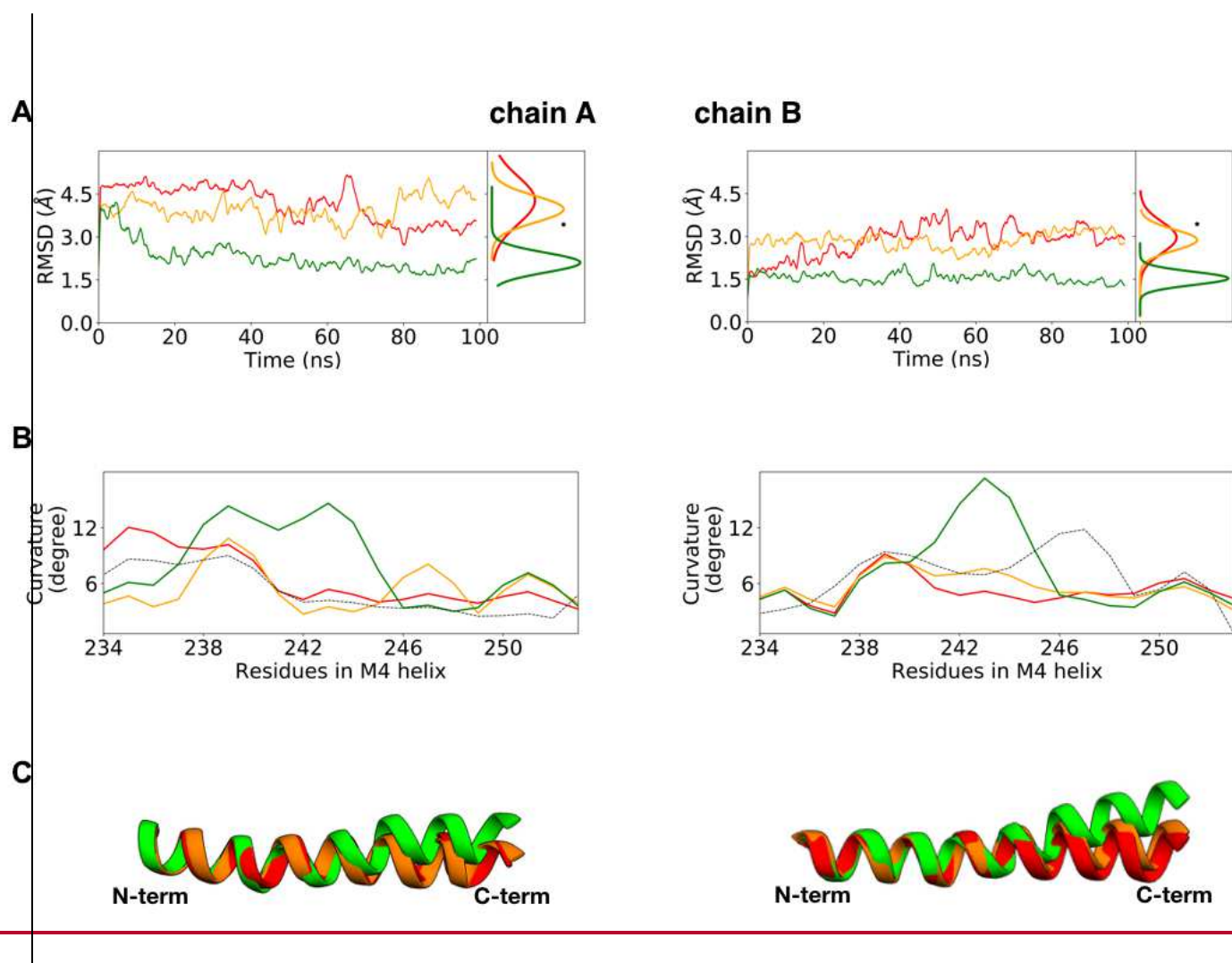
Figure S2. Conformation of helix M4, whose bending regulates the opening of the lateral fenestrations. (**A**) Root-mean square deviation of the M4 helix in chain A (left) and B (right), with respect to the crystallographic up-conformation (chain B of pdb file 4WFE). RMSD values were calculated for residues 230-257, after removal of roto-translational motions of residues 1-230. The blue asterisk represents the RMSD calculated for the crystallographic down-conformation (Chain A of 4WFE). RMSD values calculated for the different proteins are shown using different colors (p.Ala244Pro, green; p.Ala172Glu, orange; ~~WT~~ wild-type [WT], red). (**B**) Average curvature of the M4 helix in chain A (left) and B (right) along the MD trajectories of WT (red) and mutated (p.Ala244Pro, green; p.Ala172Glu, orange) KCNK4 channels. Curvature of the same helices from the crystallographic structures (4WFE, dashed lines) conformations are presented as reference (dotted). (**C**) Representative structures of helix M4 A (left) and B (right) in the simulation of the three systems (p.Ala244Pro, green; p.Ala172Glu, orange, WT, red). All data demonstrate a significantly higher bending of helix M4 in the p.Ala244Pro mutant.
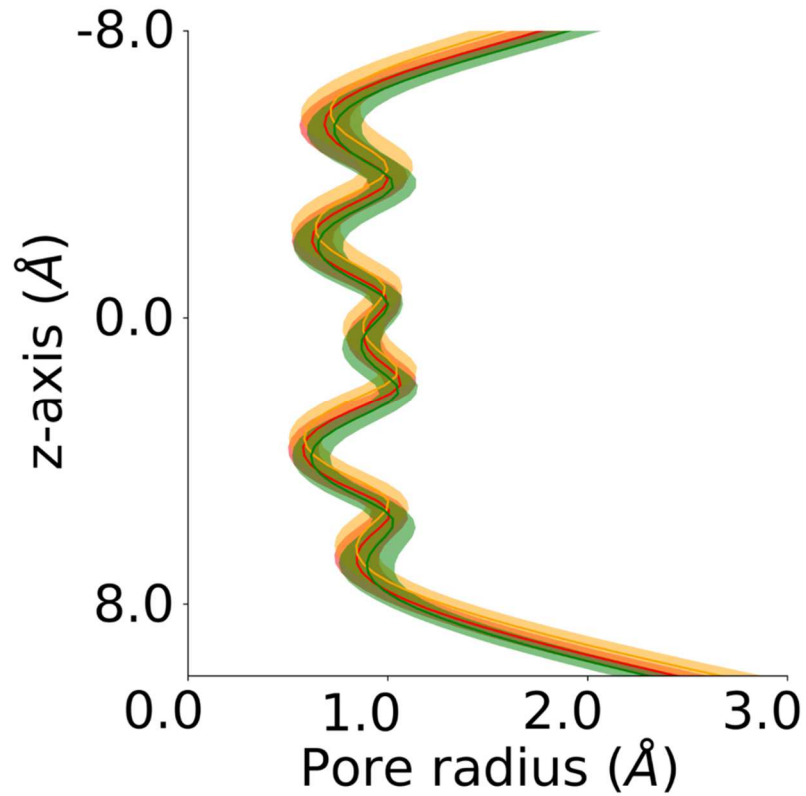
Figure S3. The selectivity filter of KCNK4 is not affected by the disease-causing p.Ala244Pro and p.Ala172Glu missense changes. Channel pore radius in the region of the selectivity filter during the MD simulations of wild-type (red), p.Ala172Glu (orange), and p.Ala244Pro (green). Solid lines and shaded areas represent the average and the standard deviation over the 100ns-long trajectories. The amino acid substitutions do not significantly affect neither the local conformation of the selectivity filter nor its flexibility.
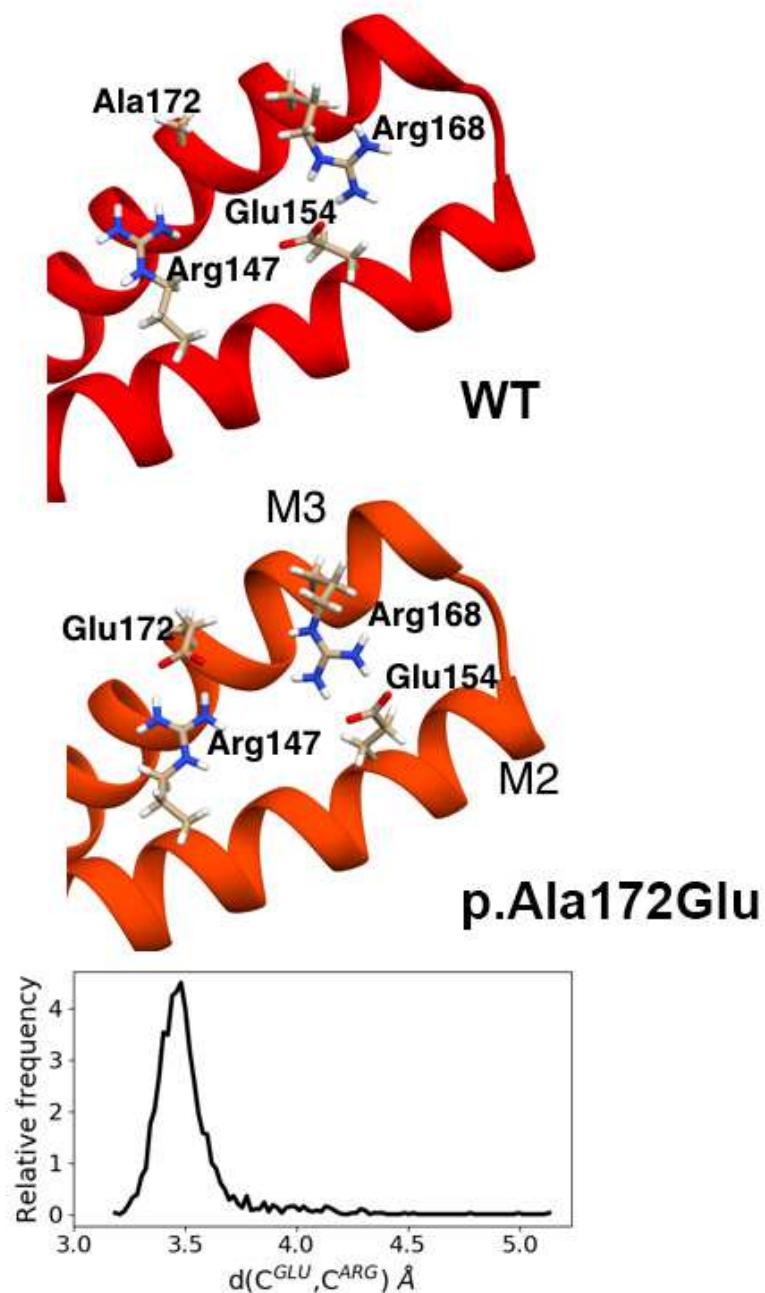
Figure S4. Structural impact of the Ala172Glu substitution. Most representative conformations of wild-type (WT) and p.Ala172Glu (A172E) in the MD trajectories, showing the formation of an additional salt-bridge between Arg[147] in M2 and Glu[172] in M3 in the simulation of the p.Ala172Glu mutant (top and middle panels). The bottom panel reports the histogram of distances between the centroids of the charged groups of the two residues in the p.Ala172Glu simulation.
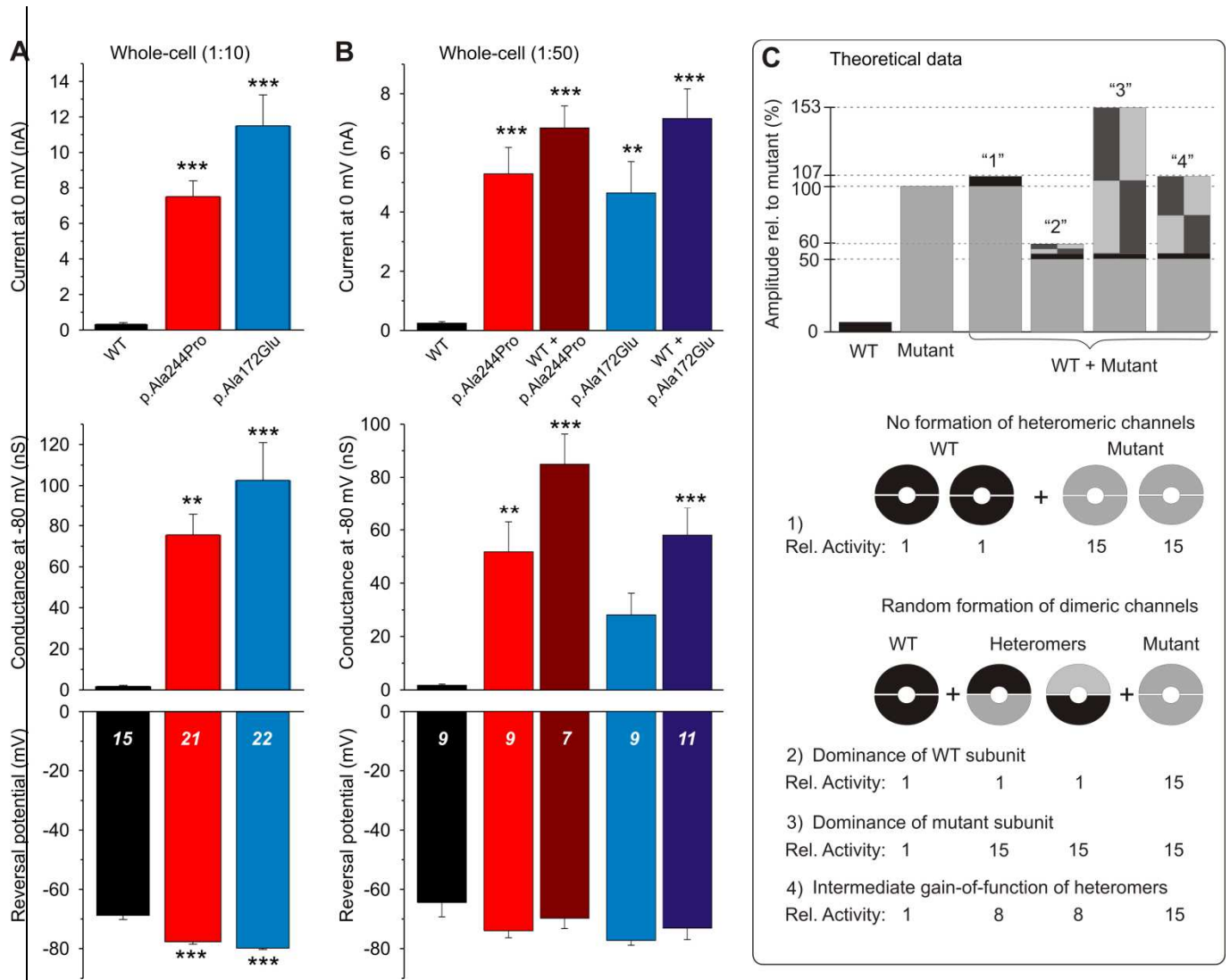
Figure S5. p.Ala244Pro (A244P) **and p.Ala172Glu** (A172E) **KCNK4 mutants increase whole-cell K+ conductance.** Analysis of whole-cell recordings from CHO cells expressing wild-type (WT) KCNK4 channels and/or the p.Ala244Pro and p.Ala172Glu KCNK4 mutants. Currents were elicited with 100-ms voltage ramps from -110 to 50 mV. Data from cells transfected with 1:10 (**A**) or 1:50 (**B**) channel cDNA predilution (1:50 + 1:50 for coexpression experiments). Data are means ± SEM (number of experiments is given in the bottom panels). Using the theoretical ramp potential, values were obtained for the current amplitude at 0 mV (top panels), the conductance at -80 mV (middle), and the potential of current reversal (as a measure of the resting membrane potential of the cell; bottom panels). One-way ANOVA with *post hoc* Bonferroni *t* testing yielded significant (** p< 0.01, *** p< 0.001) differences compared to WT data. (**C**) Theoretical estimation of the effect of additive WT and mutant KCNK4 channel subunit coexpression with an arbitrary assumption of a 15-fold increased basal activity of mutant channels compared to WT channels, and different scenarios of dimer formation and assumed activity of heteromeric channels. Despite a doubled number of channels due to a doubled amount of total channel cDNA used for transfection, the effect of additive WT and mutant subunit coexpression is expected to exceed the effect of the mutant only in the case of considerable gain-of-function of the heteromeric channels (see scenarios "3" and "4").
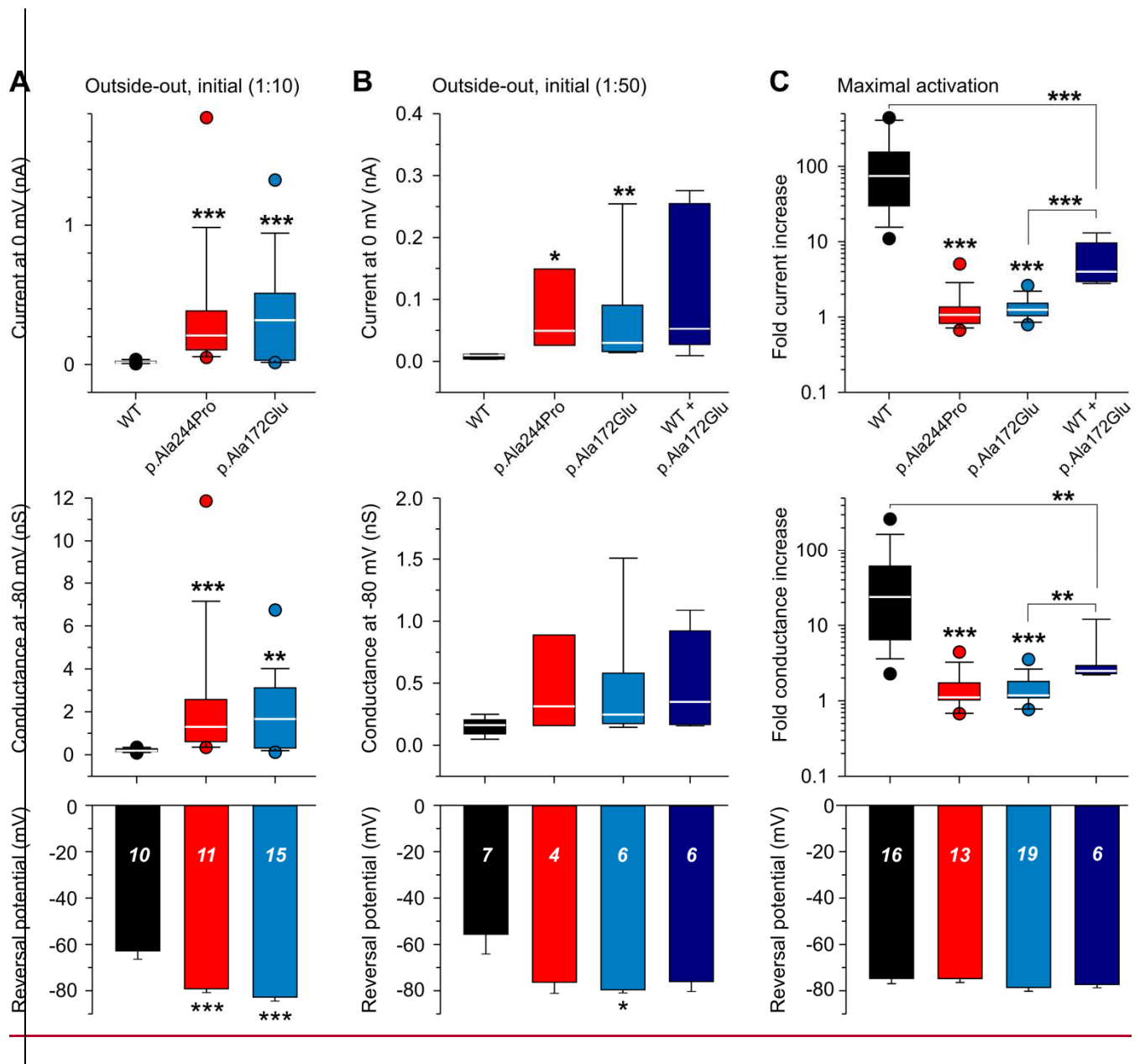
Figure S6. p.Ala244Pro ~~(A244P)~~ **and p.Ala172Glu** ~~(A172E)~~ **KCNK4 mutants increase basal K⁺ conductance in unstimulated outside-out patches and show impaired response to mechanical stimulation.** Analysis of experiments with intermittent pressure stimulation in the outside-out patch-clamp configuration from CHO cells expressing wild-type (WT) or mutant KCNK4 channels. Membrane currents were recorded during 100-ms voltage ramps from -110 to 50 mV. (**A**) and (**B**) Data obtained shortly after forming the outside-out configuration and before the first pressure stimulation. Data were separately analyzed for cells transfected with 1:10 (**A**) or 1:50 (**B**) prediluted channel cDNA. For coexpression of WT and p. Ala172Glu KCNK4 channel subunits, cDNAs were used in a 1 to 1 ratio (1:50 + 1:50). Values were obtained for the current amplitude at 0 mV (top panels), the conductance at -80 mV (middle), and the potential of current reversal (bottom panels). Current amplitude and conductance data are given as box plots (Cleveland method; whiskers indicate 10/90 percentiles and points indicate 5/95 percentiles, they are lacking for groups with a small number of experiments) and the reversal potential bars show means ± SEM (given number of experiments also applies to the current and conductance data). (**C**) Analysis of maximal pressure (and time) -induced changes in the recorded membrane currents before patch rupture (indicated by a shift of the reversal potential towards 0 mV). Combined data from experiments using

1:10 or 1:50 cDNA predilution for transfection. Fold current increase and fold conductance increase were calculated as ratio of the values obtained with maximal pressure stimulation to the initial values without stimulation. Please note the logarithmic scale of these two parameters. Positive pressure resulted in significant increases in current amplitudes at 0 mV for WT (fold current increase: median = 74.4, $p < 0.001$), p.Ala172Glu (fold current increase: median = 1.243; $p < 0.001$) and coexpressed WT + p.Ala172Glu KCNK4 (factor current increase: median = 4.00, $p < 0.001$), but not for p.Ala244Pro KCNK4 channels (fold current increase: median = 1.065, $p = 0.168$). The reversal potential (bottom panel) was determined during maximal stimulation. (**A-C**) Nonparametric statistical analysis was performed for current and conductance data: if Kruskal-Wallis tests yielded significant differences between groups (ANOVA on ranks for WT, p.Ala244Pro and p.Ala172Glu) and *post hoc* Dunn's testing yielded significant differences compared to WT data, the individual significance levels were determined with the Wilcoxon-Mann-Whitney test (* p< 0.05, ** p< 0.01, *** p< 0.001). Normalized WT + p.Ala172Glu coexpression data ("Fold current increase" and "Fold conductance increase") were tested for differences to WT data and to p.Ala172Glu data with the Wilcoxon-Mann-Whitney test. Reversal potential values were tested for statistically significant differences with one-way ANOVA and *post hoc* Bonferroni *t* testing. Significant differences compared to WT data are indicated (* p< 0.05, *** p< 0.001).
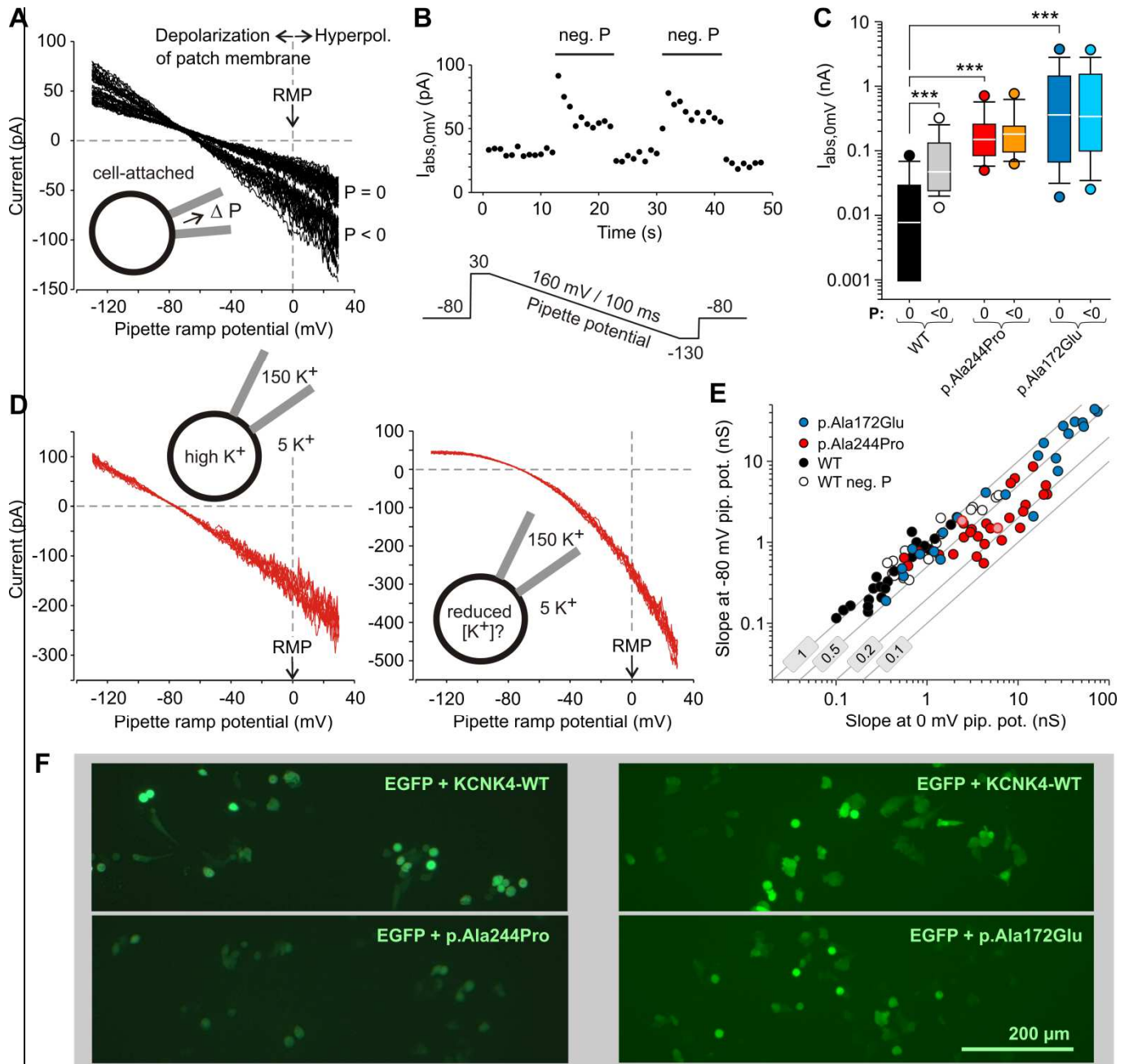
Figure S7. Cell-attached current recordings ~~were performed~~ **on CHO cells expressing either wild-type (WT), p.Ala244Pro** ~~(A244P)~~ **or p.Ala172Glu** ~~(A172E)~~ **KCNK4 channels.** Transfection with 1:10 predilution of channel cDNA. Currents were repeatedly elicited with the ramp protocol shown below **B** with intermittent application of negative pressure through the patch pipette. Please note that positive pipette potentials hyperpolarize, and negative pipette potentials depolarize the patch membrane. (**A**) I/V-plot of current traces recorded from a cell expressing WT KCNK4 channels. (**B**) Time course of the absolute amplitude of the inward current measured at 0 mV pipette potential ($I_{abs,0mV}$); same experiment as shown in **A**. (**C**) Comparative analysis of cell-attached current recordings without (P = 0) and with (P < 0) negative pressure stimulation to cells expressing WT or mutant KCNK4 channels. Box plot (Cleveland method; whiskers indicate 10/90 percentiles and points indicate 5/95 percentiles) of the inward current amplitude at 0 mV ($I_{abs,0mV}$). Statistical difference in basal current amplitudes was tested with ANOVA on ranks (Kruskal-Wallis test); *post-hoc* Dunn`s testing yielded significant differences compared to WT data and the individual significance levels were determined with the Wilcoxon-Mann-Whitney test (* $p < 0.05$, ** $p < 0.01$, *** $p < 0.001$). Negative pressure significantly increased currents in experiments on WT channels (Wilcoxon signed rank test; ***$p < 0.001$, n =

21), but not in experiments on p.Ala244Pro (p = 0.055, n = 19) or p.Ala172Glu (p = 0.595, n = 19) KCNK4 channels. (**D**) I/V-plots from current traces recorded from two different cells expressing p.Aala244Pro KCNK4 channels demonstrating minimal (left panel) or pronounced (right panel) inward rectification. (**E**) To visualize the variable degree of inward rectification, the conductance (slope of the I/V plot) at -80 mV was plotted against the conductance at 0 mV pipette potential for all individual experiments on WT and mutant KCNK4 channels. The plot also contains data on pressure-activated WT channels. Data points close to the line marked with "1" (i.e. identical slope values at 0 and at -80 mV pipette potential) result from a linear I/V relation (no rectification). The line marked with 0.2 (ratio of the slope at -80 mV to the slope at 0 mV is 1:5) indicates strong inward rectification. The two data points filled light red correspond to the experiments shown in **D**. Strong inward rectification suggested to result from internal K^+ depletion most often occurred in experiments on p.Ala244Pro KCNK4 channels. (**F**) EGFP fluorescence of CHO cells 24h after transfection with EGFP plus either WT or p.Ala244Pro *KCNK4* cDNA (micrographs on the left) and EGFP fluorescence 48h after transfection with EGFP plus either WT or p.Ala172Glu *KCNK4* cDNA (micrographs on the right). Cells expressing the p.Ala244Pro KCNK4 mutant showed less often bright EGFP fluorescence than cells expressing the WT channel. This effect was less apparent for the p.Ala172Glu KCNK4 channel mutant.